NTNU

Norwegian University of
Science and Technology

Modelling flood events in the Arno River and the interaction with the infrastructures in the city of Florence using REEF3D

Niccolò Nuti

Civil and Environmental Engineering
Submission date: October 2018
Supervisor: Hans Sebastian Bihs, IBM
Co-supervisor: Arun Kamath, IBM

Norwegian University of Science and Technology
Department of Civil and Environmental Engineering

School of Engineering

Master of Science
in
Civil and Environmental Engineering

Modelling flood events in the Arno River and the interaction with the infrastructures in the city of Florence using REEF3D

Supervisors:
Hans Bihs
Luca Solari
Arun Kamath
Tobias Martin

Candidate:
Niccoló Nuti

Abstract

The urban part of Florence is still at hydraulic risk because of the interaction between the river flow and the structures like bridges and weirs. The purpose of this work is to investigate the stability of the old structures and to reduce the hydraulic risk in the urban part, so as to avoid dramatic situations like the flood event happened in 1966. The river reach analysed counts four bridges (Ponte Vecchio, Santa Trinita, alla Carraia and Vespucci) and one weir (Pescaia di Santa Rosa).The work is realised through the open source hydrodynamic software REEF3D. In particular, two approaches are used: REEF3D::SFLOW and REEF3D::CFD. The first is focused on understanding the overall flow pattern of the river, while the second is applied to examine more in depth the three-dimensional water behaviour and the hydrodynamic parameters involved.

Acknowledgments

I would like to express my heartfelt thanks to my Italian supervisor Prof. Eng. Luca Solari that made my experience in Norway possible. I would also like to thank my NTNU supervisor Prof. Eng. Hans Bihs that gave me the chance and the means to work on my project. Special thanks to the REEF3D team: Arun, Tobias and Weizhi, who were always available to help me whenever I encountered obstacles on the way. Particular gratitude is reserved to my parents, Fabio and Manuela, who are always believing in my possibilities and encouraging me. My sister Martina and my girlfriend Denise deserve special thanks, for giving me the support and the affection I needed away from home. I would like also to thank the group of friends P.B., the friends from university and all the colleagues and flatmates in Norway. Each one contributed to enrich my experience abroad.

Contents

List of Figures

List of Tables

List of Symbols

ρ	density [Kg/m^3]
f_i	mass forces [N]
v_i	velocity [m/s]
p_i	pressure [N/m^2]
μ	fluid dynamic viscosity [Ns/m^2]
ν	fluid cinematic viscosity [m^2/s]
i, j, k	vectors along the x, y and z-direction
T	time [s]
g	gravitational acceleration
V_i	averaged velocity [m/s]
$v_i' v_j'$	Reynolds stresses
w_1, w_2, w_3	WENO stencil weights
$\tilde{w}_1, \tilde{w}_2, \tilde{w}_3$	WENO stencil weights determiners
β_1, β_2, β_3	WENO stencil smoothness indicators
$\bar{k}$	kinetic energy
δ_{ij}	Kronecker delta
ν_T	kinematic eddy viscosity
$\bar{D}_{ij}$	velocity deformation tensor
u^*	intermediate velocity
$\phi(\vec{x}, t)$	level set function

Q	water discharge [m^3/s]
h	height of water level [m]
n	Manning's roughness coefficient
Fr	Froude number
U	uniform motion velocity [m/s]
y	water depth [m]
y_{cr}	critical water depth [m]
E	specific energy
E_{min}	minimal specific energy

Chapter 1

Introduction

1.1 General

The rivers network represents only a small percentage of the water on earth. Nevertheless, the presence of a stream has always meant *life*. Since the beginning of the human history, the ancient civilizations grew up in proximity of a water source. It was the base for survival, agriculture, irrigation and an easy way to move and trade. Over time, in particular after the industrialisation, water was also used by factories to feed their internal processes. Only at a later stage, the potential of the water flow was directed to the electric energy production. In the meanwhile, the increase of the population and the need of new buildings led to the urbanisation of wide and wild areas neighbouring the rivers. Nowadays, the lack of flood plains that are proper natural outlets and the occurrence of extreme events increase the number of inundations and of hydraulic problems turning the rivers into potential risks. Hence, the need to reducing the hydraulic hazard and to creating efficient systems of prevention.
The case of study is located in Italy which territory is particularly subject to flood events. The terrain morphology and the thick rivers network together with the wide urbanisation represent a constant risk, mitigated only by detention basins.
In recent years, the improvements achieved in numerical modelling can be applied to real cases. An evaluation through mathematical models can help analysing and understanding more in depth the hydraulic behaviour of the rivers and to allow the engineer to identify possible solutions.

1.2 Present Work

The urban part of Florence is still at high hydraulic risk because of the interaction between the Arno river flow and the structures like bridges and weirs. The International Technical Scientific Committee (ITSC) recently reviewed and evaluated the

potential flooding risk in the city of Florence [13]. The main observation reported from ITSC is the following: *"Florence remains at risk of significant flooding which increases every day. The question is not related to the occurrence of a possible flood of the magnitude of 1966 or greater, but when it will happen. In fact, the actual level of protection existing in Florence does not provide the risk reduction needed for this city and it is not of a degree that can be considered appropriate to the citizens and cultural heritage that rest within the city."*. This feeds, in part, the motivations for the present work.
To this day, the water behaviour is unknown and dangerous situations could take place during extreme events. In the surrounding area, the flood plains have been gradually replaced with buildings and constructions from human activity, so that water has to be necessarily contained within the river banks. An important flood event may result in a risk for the citizens living in the historical city centre and the artistic heritage located all around the area.
The presence of old structures, such as the Ponte Vecchio and the Santa Rosa weir, deserve a particular attention due to their historical values and the effects caused to the natural river flow.
A throughout hydrodynamic analysis aiming at verifying the stability of these old structures is essential to reduce the flood risks and represents the objective of the present work. The purpose is to check the stability of the old structures and to reduce the hydraulic risk through:

- Investigating the two-dimensional overall flow pattern and showing the flux lines;
- Investigating the three-dimensional water behaviour along the river reach;
- Analysing and investigating the three-dimensional water behaviour under the Ponte Vecchio arches as well as calculating the forces involved.

The advantage of using a 3-dimensional model consists in collecting a higher level of information in terms of hydrodynamic parameters. More specifically, the water motion can be distributed in the three dimensions so that, for example, the vortexes generated by the turbulence can be identified and inspected in the whole space. Models such as 2-dimensional and 1-dimensional are based on several assumptions (motion along 2 or 1 directions, hydrostatic distribution of pressure, etc.) and exclude phenomena characterising the real river flow.
The above mentioned issues will be studied through the creation of a simulation setup and then a simulation with the open-source hydrodynamic software REEF3D, which is used for a wide range of applications within hydraulic and marine engineering [7] [22] [18] [20] [6] [2] [14]. The software will show the complex free surface features involved along the flow of the river through the old structures extracting information

on velocity vectors, flux lines and other hydrodynamic parameters.
The first part of this work provides the numerical model overview including the governing equations, the turbulence model and the discretization methods. The second part describes the geographical position of Florence, its hydraulic history and the data collected on the river reach in the urban part. In the third part, some experimental cases analysing the flow around the piers and over a weir are introduced in order to validate the software performance. In the last part, the case study is presented. The results obtained from the simulations are discussed and analysed to get a in-depth understanding of the flow phenomena in the Arno river.

1.3 Objectives

The objectives of the present work can be summarised as follows:

- Create a 2D model of the Arno river reach.
- Validate the REEF3D software for weir and double pier cases through experimental data.
- Create a 3D model of a flow around an arch bridge.
- Create a 3D model of the Arno river reach and simulate with various discharges.
- Use the field measurements to validate the simulations and discuss the results obtained.

Chapter 2

Numerical Model

The software used for the present work is REEF3D, an open-source hydrodynamics program developed by the Norwegian University of Science and Technology (NTNU). The implementation of REEF3D leads to solve a wide range of applications [19] [24] [21], as the followings:

- numerical wave tank
- wave forces
- coastal modelling
- sediment transport
- open channel flow
- dam break

The software is able to treat some flow problems through the SFLOW, NSEWAVE and CFD (Computational Fluid Dynamics) approaches. This chapter shall be responsible for giving a general overview of the numerical model regarding the CFD approach. As reported by [3], the physics related to any fluid flow is governed by the Newton's fundamental principles:

- mass is conserved (1^{st} principle)
- F=ma (2^{nd} principle)
- energy is conserved (3^{rd} principle)

These principles can be written as mathematical equations, usually as partial differential equations: Navier-Stokes (N-S) equations. The objective of the computational fluid dynamics is to replace the equations with numbers that, progressing in space and time, contribute to define the numerical description of the flow field.

2.1 Governing Equations

REEF3D is based on the Reynolds Averaged Navier-Stokes (RANS) equations. Before investigating further, some details about the origin of the RANS equations are needed. The starting equations are the continuity and momentum equations:

$$v_{i,i} = 0 \tag{2.1}$$

$$\rho\left(f_i - v_{i,T} - v_j v_{i,j}\right) = p_{,i} - \mu v_{i,jj} \tag{2.2}$$

in which:

- ρ= density
- f_i = mass forces
- $v_{i,T}$ = temporal variation of velocity
- $v_j v_{i,j}$ = spatial variation of velocity or convection term
- $p_{,i}$ = pressure term
- μ= dynamic viscosity
- $v_{i,jj}$ = Laplace operator
- $\mu v_{i,jj}$ = viscous term or diffusion

In (2.2), $v_j v_{i,j}$ is the non-linear term.
The turbulence cannot be resolved completely so it needs to be modelled, typically using time averaged values. This is possible with the Reynolds decomposition.
If considering to measure the velocity parameter v_i of the water flow in a river over the time, the value of the instantaneous velocity always changes during time. Displaying the measurements in a Cartesian coordinate system with time on the x-axis and velocity on the y-axis, the result is a sawteeth graph as shown in Fig. 2.1.

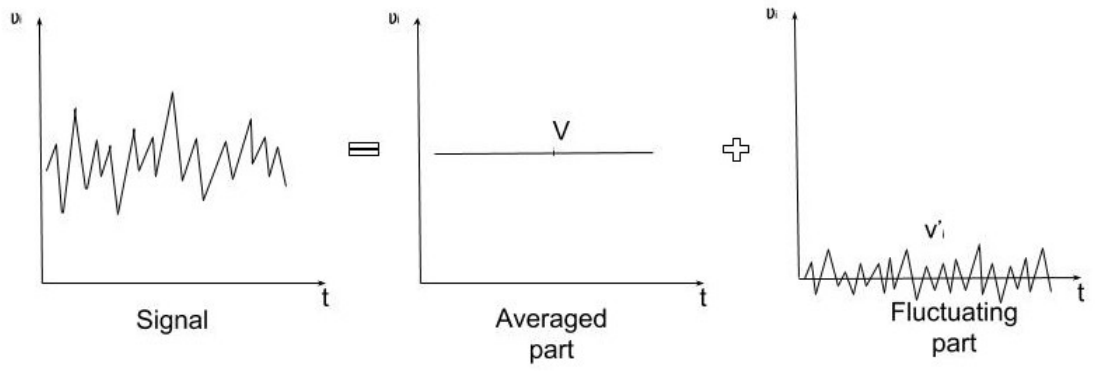

Figure 2.1: Reynolds decomposition of the velocity over the time

The original signal is composed by the averaged and the fluctuating part.
Through the Reynolds decomposition and through the implementation of the time average in (2.1) and (2.2), it is possible to express the RANS equations:

$$V_{i,i} = v'_{i,i} = 0 \tag{2.3}$$

$$\rho\left(f_i - V_{i,T} - V_j V_{i,j} - \left(\overline{v'_i v'_j}\right)_{,i}\right) = P_{,i} - \mu V_i, jj \tag{2.4}$$

in which:

- ρ= density
- f_i = mass forces
- $V_{i,T}$ = temporal variation of the averaged velocity
- $V_j V_{i,j}$ = spatial variation of the averaged velocity
- $\left(\overline{v'_i v'_j}\right)$ = turbulent fluctuations of velocity
- $P_{,i}$ = pressure term
- μ= dynamic viscosity
- $V_{i,jj}$ = Laplace operator
- $\mu V_{i,jj}$ = viscous term or diffusion

The turbulent fluctuations of velocity $\overline{v'_i v'_j}$ are the Reynolds stresses. Even if the previous transformations make it possible to obtain averaged terms, the Reynolds stresses still remind the turbulent regime derived from the non-linear term.

2.2 Discretization Method

The RANS equations are partial differential equations. Analytical methods use closed-form expressions in which the dependent variables, vary continuously in the domain [3]. Unfortunately these methods can not be applied in this case. Hence, numerical methods are needed, allowing the transition from a continuous to a discrete problem. It means that the numerical solutions can be computed only in specific points of the domain on which a Cartesian grid is introduced. The unknown variables, like velocity and pressure, are not located in the same grid points. In order to facilitate the ease of the calculations, a staggered grid is used as shown in the Fig. 2.2.

There are several discretization methods, such as:

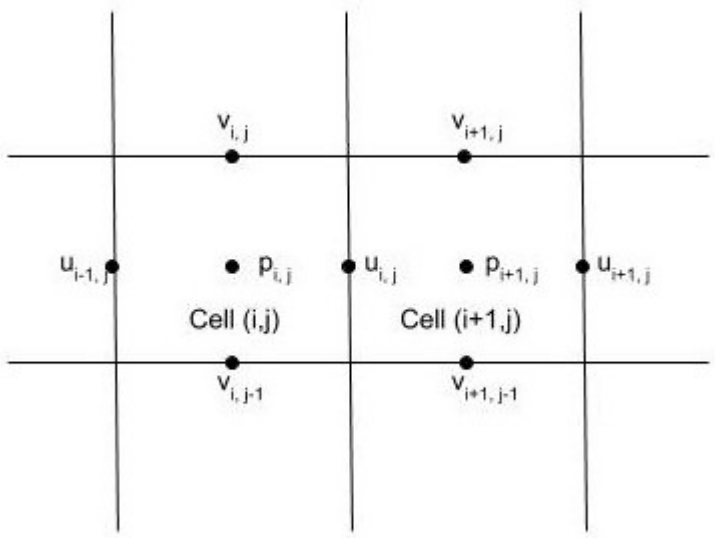

Figure 2.2: Staggered grid

- Finite Volume Method (FVM)
- Finite Elements Method (FEM)
- Finite Difference Method (FDM)

The Finite Volume Method integrates the RANS equation over a volume defined by control volumes in the grid. Then the transformation from the volume to the surface integrals makes it possible to calculate the fluxes through the surfaces of the cells. The method is conservative, meaning that, if convergent, it leads to the right solution of the system [31].

The Finite Difference Method is based on the approximation of the equations using the Taylor series and it is more suitable for an equidistant Cartesian grid. In particular the continuity and momentum equations are replaced with a system of algebraic equations to be solved in each point of the grid [3].
The method used in this work belongs to the finite difference framework with a high-order temporal and spatial discretization.

2.2.1 Convection Discretization

The convective term of the RANS equations is discretized with the 5th order Weighted Essentially Non-Oscillatory (WENO) scheme. The WENO schemes are formulated on the base of the Essentially Non-Oscillatory (ENO) schemes developed for the first time by Harten [16]. These schemes search for the smoothest stencil to estimate the fluxes at the cell boundaries with a high order accuracy and prevent oscillations [17]. The difference introduced in the WENO schemes is that the fluxes are not approximated with only one of the candidate stencils but with a compound of all. Each stencil has a proper weight that influences the final approximation of the flux.
The approximation of the derivative $f(u)_x$ through a conservative finite difference spatial discretization could be written as [28]:

$$f(u)_x|_{x=x_j} \approx \frac{1}{\Delta x}\left(\hat{f}_{j+\frac{1}{2}} - \hat{f}_{j-\frac{1}{2}}\right) \tag{2.5}$$

where $\hat{f}_{j+\frac{1}{2}}$ is the numerical flux.
In the 5th order WENO scheme the flux is given by:

$$\hat{f}_{j+\frac{1}{2}} = w_1\hat{f}^{(1)}_{j+\frac{1}{2}} + w_2\hat{f}^{(2)}_{j+\frac{1}{2}} + w_3\hat{f}^{(3)}_{j+\frac{1}{2}} \tag{2.6}$$

where $\hat{f}^{(i)}_{j+\frac{1}{2}}$ are three third order stencils fluxes on three different stencils given by:

$$\begin{aligned}
\hat{f}^{(1)}_{j+\frac{1}{2}} &= \frac{1}{3}f\left(u_{j-2}\right) - \frac{7}{6}f\left(u_{j-1}\right) + \frac{11}{6}f\left(u_j\right) \\
\hat{f}^{(2)}_{j+\frac{1}{2}} &= -\frac{1}{6}f\left(u_{j-1}\right) + \frac{5}{6}f\left(u_j\right) + \frac{1}{3}f\left(u_{j+1}\right) \\
\hat{f}^{(3)}_{j+\frac{1}{2}} &= \frac{1}{3}f\left(u_j\right) - \frac{5}{6}f\left(u_{j+1}\right) - \frac{1}{6}f\left(u_{j+2}\right)
\end{aligned} \tag{2.7}$$

and the non-linear weights w_i are given by

$$w_1 = \frac{\tilde{w}_1}{\sum_{k=1}^{3}\tilde{w}_k}, w_2 = \frac{\tilde{w}_2}{\sum_{k=1}^{3}\tilde{w}_k}, w_3 = \frac{\tilde{w}_3}{\sum_{k=1}^{3}\tilde{w}_k} \tag{2.8}$$

and

$$\tilde{w}_1 = \frac{1}{10}\frac{1}{(\varepsilon+\beta_1)^2}, \tilde{w}_2 = \frac{3}{5}\frac{1}{(\varepsilon+\beta_2)^2}, \tilde{w}_3 = \frac{3}{10}\frac{1}{(\varepsilon+\beta_3)^2} \tag{2.9}$$

and the smoothers indicators β_1, β_2 and β_3 are given by:

$$\begin{aligned}
\beta_1 &= \frac{13}{12}\left(f\left(u_{j-2}\right) - 2f\left(u_{j-1}\right) + f\left(u_j\right)\right)^2 + \frac{1}{4}\left(f\left(u_{j-2}\right) - 4f\left(u_{j-1}\right) + 3f\left(u_j\right)\right)^2 \\
\beta_2 &= \frac{13}{12}\left(f\left(u_{j-1}\right) - 2f\left(u_j\right) + f\left(u_{j+1}\right)\right)^2 + \frac{1}{4}\left(f\left(u_{j-1}\right) - f\left(u_{j+1}\right)\right)^2 \\
\beta_3 &= \frac{13}{12}\left(f\left(u_j\right) - 2f\left(u_{j+1}\right) + f\left(u_{j+2}\right)\right)^2 + \frac{1}{4}\left(3f\left(u_j\right) - 4f\left(u_{j+1}\right) + f\left(u_{j+2}\right)\right)^2
\end{aligned} \tag{2.10}$$

ε is a coefficient to evade the denominator going to zero and it is usually assumed ε=10^{-6}.

2.3 Time Discretization

In REEF3D, different time discretization methods are applicable. As regards the explicit ones, it is possible to consider:

- 2^{nd}order Adams-Bashforth
- 2^{nd} and 3^{rd}order TVD Runge-Kutta
- 3^{rd} and 4^{th}order Runge-Kutta

In order to guarantee the accuracy and the stability of the time discretization, the explicit 3rd order TVD Runge-Kutta scheme is recommended and, therefore, used in this thesis. As reported by Shu [27], the advantage of TVD approach can be expressed as a high-order accuracy in smooth regions without oscillations that could be caused due to the presence of discontinuities. Considering a generic variable ϕ, an implementation of the 3rd order TVD Runge-Kutta scheme reads [7]:

$$\begin{aligned}
\phi^{(1)} &= \phi^n + \Delta t L\left(\phi^n\right) \\
\phi^{(2)} &= \frac{3}{4}\phi^n + \frac{1}{4}\phi^{(1)} + \frac{1}{4}\Delta t L\left(\phi^{(1)}\right) \\
\phi^{(n+1)} &= \frac{1}{3}\phi^n + \frac{2}{3}\phi^{(2)} + \frac{2}{3}\Delta t L\left(\phi^{(2)}\right)
\end{aligned} \tag{2.11}$$

2.4 Turbulence Model

As briefly discussed in the section 2.1, the turbulence is included in the momentum equation of the RANS through the Reynolds stresses.
The turbulent closure problem is solved with the Boussinesq approximation that replaces the Reynolds stresses:

$$-\overline{v_i' v_j'} = -\frac{2}{3}\bar{k}\delta_{ij} + 2\nu_T \bar{D}_{ij} \tag{2.12}$$

where

- $\bar{k}$ = kinetic energy of the turbulent fluctuations
- δ_{ij} = Kronecker delta
- ν_T = kinematic eddy viscosity
- $\bar{D}_{ij}$ = mean velocity deformation tensor

REEF3D has several models to manage the turbulence like the k-ϵ and the k-ω models, belonging to the two-equations models framework. The advantage of using these models is the adaptability to a turbulent flow in which the turbulence structure is unknown [34].

- k-ω model

$$\nu_T = \frac{k}{\omega} \tag{2.13}$$

$$k_{,T} + u_j k_{,j} = \tau_{ij} u_{i,j} - \beta^* k\omega + \left[\left(\nu + \sigma^* \frac{k}{\omega}\right) k_{,j}\right]_{,j} \tag{2.14}$$

$$\omega_{,T} + u_j \omega_{,j} = \alpha \frac{\omega}{k} \tau_{ij} u_{i,j} - \beta\omega^2 + \frac{\sigma_d}{\omega} k_{,j}\omega_{,j} + \left[\left(\nu + \sigma \frac{k}{\omega}\right) \omega_{,j}\right]_{,j} \tag{2.15}$$

with

$$\alpha = \frac{13}{25}, \qquad \beta = \frac{3}{40}, \qquad \beta^* = \frac{9}{100}, \qquad \sigma = \frac{1}{2}, \qquad \sigma^* = \frac{3}{5} \tag{2.16}$$

- k-ϵ model

$$\nu_T = C_\mu \frac{k^2}{\epsilon} \tag{2.17}$$

$$k_{,T} + u_j k_{,j} = \tau_{ij} u_{i,j} - \epsilon + \left[\left(\nu + \frac{\nu_T}{\sigma_k}\right) k, j\right]_{,j} \tag{2.18}$$

$$\epsilon_{,T} + u_j \epsilon_{,j} = C_{\epsilon 1} \frac{\epsilon}{k} \tau_{ij} u_{i,j} - C_{\epsilon 2} \frac{\epsilon^2}{k} + \left[\left(\nu + \frac{\nu_T}{\sigma_\epsilon} \right) \epsilon_{,j} \right]_{,j} \tag{2.19}$$

with

$$C_{\epsilon 1} = 1.44, \qquad C_{\epsilon 2} = 1.92, C_\mu = 0.09, \qquad \sigma_k = 1.00, \qquad \sigma_\epsilon = 1.3 \tag{2.20}$$

In this project, the k-ϵ model is chosen

2.5 Pressure

In order to solve the RANS, the pressure term included in the momentum equation has to be calculated. The used method in REEF3D is the Projection Method developed by Chorin in 1968 [9].
First, an intermediate velocity u^* has to be computed ignoring the pressure term, so that the momentum equation can be written as:

$$\left(u^* - u_i^n\right)_{,T} + u_j^n u_{i,j}^n = \left[\nu(\phi^n) \left((uU_i^n)_{,j} + u_{j,i}^n \right)\right]_{,j} + g_i \tag{2.21}$$

Then, it is possible to calculate the velocity in the next time step through the Poisson equation for the pressure.

$$\left(u_i^{n+1} - u_i^*\right)_{,T} + \frac{1}{\rho(\phi^n)} \left(p_{,i}^{n+1}\right) = 0 \tag{2.22}$$

The Poisson equation is expressed as:

$$\left(\frac{1}{\rho(\phi^n)} P_{,i} \right)_{,i} = -\frac{1}{\Delta T} U_{i,i}^* \tag{2.23}$$

2.6 Free Surface Model

REEF3D is based on a two-phase model. The Level Set Method has the aim of capturing the moving fluid free surface on a fixed mesh. The key aspect is the definition of a function ϕ and capturing its evolution. The zero-level-set corresponds to the interface between the two phases [1]. The level-set function ϕ has the following properties:

$$\phi(\vec{x}, t) \begin{cases} > 0 \;\; if \;\; \vec{x} \in phase1 \\ = 0 \;\; if \;\; \vec{x} \in \Gamma \\ < 0 \;\; if \;\; \vec{x} \in phase2 \end{cases} \tag{2.24}$$

The motion of the level-set function in space and time is described as:

$$\phi_{,T} + u_j \phi_{,j} = 0 \tag{2.25}$$

Equation 2.25 has been discretised in time and space. For the time, the 3^{rd} order TVD Runge-Kutta scheme is commonly used, while for the space the WENO scheme is recommended.
During the convection of the level set function, it could misplace its distance property. In order to elude this problem, the function is reinitialized at the beginning of each time step. The reinitialization is based on the following partial differential equation [29]:

$$\phi_{,T} + S(\phi)(|\phi_{,j}| - 1) = 0 \tag{2.26}$$

2.7 Solver

The linear systems can be solved through two schemes:

- Direct Elimination Methods
- Iterative Methods

The first are mainly based on the Gauss Elimination technique that works through direct operations on the matrix rows to facilitate the solution of the system [30]. An example is the LU scheme.
The second are commonly used to deal with huge systems. Their usage is preferable considering the accuracy, the efficiency and the capability to treat non-linear systems. In the context of the iterative solver, HYPRE is the software library chosen for the solution of the equation systems. It allows the user to manage advanced parallel preconditioners [12].
In the REEF3D framework, there are several iterative solvers that can be applied to the velocities and the scalars. The Bi-Conjugate Gradient Stabilized (BiCGstab) method with the Jacobi-Scaling preconditioner proves to be the most effective. The Poisson equation is solved with the BiGCstab of HYPRE Struct, appropriate for scalar applications on rectangular grids. The preconditioner used for the Poisson equation is the PFMG which is a parallel multigrid solver.

2.8 Boundary Treatment

The creation of a Cartesian grid sets up the field on which the numerical model is implemented. The presence of irregular solid boundaries on the grid needs to be used along with the application of an immersed boundary scheme [7]. The one used in

REEF3D is the Ghost Cell Immersed Boundary Method (GCIBM).
The use of the ghost cells is specific and quite efficient. The ghost cells are imaginary cells inside the solid [5]. The boundary conditions do not need to be calculated explicitly since they are included implicitly into the ghost cells.

Chapter 3

Study Case: Arno River

The following chapter describes the features of the Arno River and, in part, of the city of Florence. An overview about the characteristics of the river, the previous analytical works and the data are presented in the next sections.

3.1 River Framework

3.1.1 River Characteristics

As reported in [33], Arno is the main river in the Tuscany region and one of the most important in Italy. It originates from Mount Falterona which belongs to the Appennine mountain chain located at the border between the regions of Tuscany and Emilia Romagna. The source, called Capo d'Arno, is placed at the height of 1358 m above the sea level. The total lenght is 241 km. The river passes by some cities like Florence, Empoli and Pisa and flows into the Tirrenian Sea in the proximity of Bocca d'Arno. The year averaged discharge is 110 m^3/s.
In spite the significant catchment area, Arno is classified as a river with a torrential behaviour because of its morphological structure and because it represents an important resource for agriculture and industry. In fact the river can change from an almost dry condition to a flood event in a very short time.
During the centuries, the area concerned by the river was subject to several flood events that changed the way of living of its inhabitants, but also the morphology of the river. The most catastrophic events were in the years 1333, 1547, 1557, 1844 and 1966 [32]. A particular section is dedicated to this last one.
In order to prevent flood events, in the last decades, some detention basins were built. The most important, regarding the costs and the usage, is the Bilancino lake. The hydraulic structure of Bilancino ensures storing the excess of water during the flood periods and to releasing it during the dry periods back to the river.

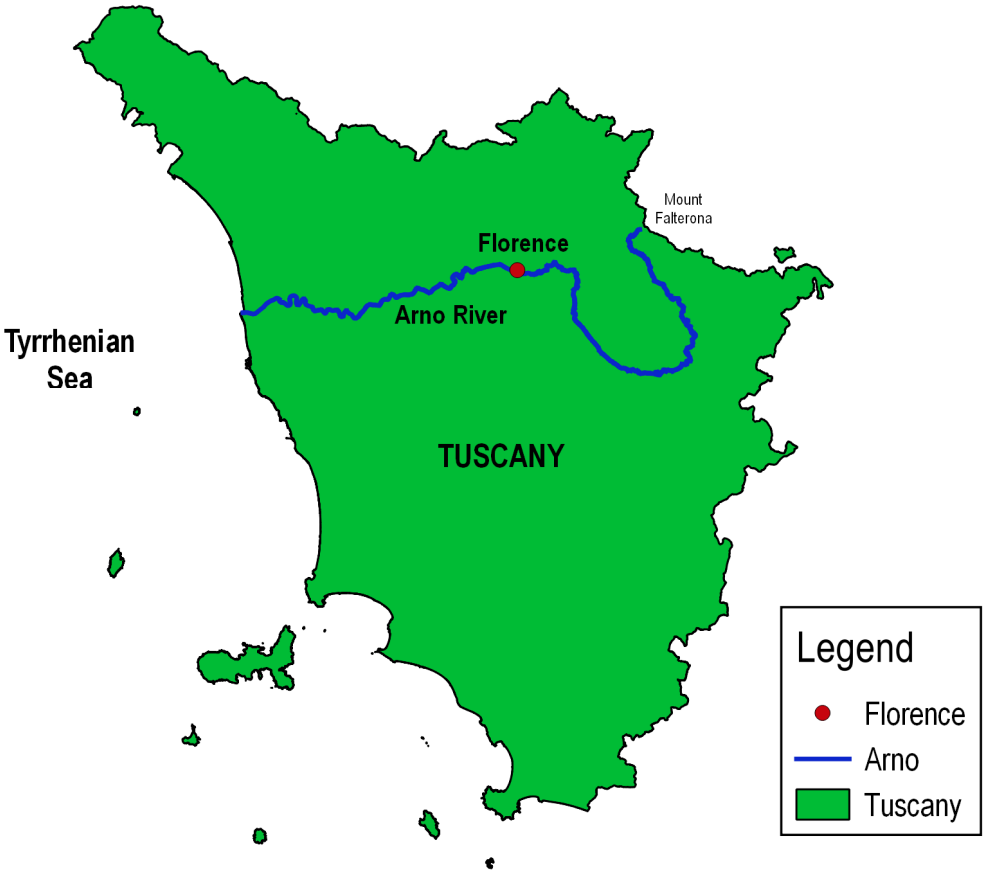

Figure 3.1: Tuscany and Arno river

Table 3.1: Main characteristics of the Arno river

Morphologic characteristics	**Value**
River length	241 Km
Mean slope	0.5-0.6%
Basin mean Height	353 m.a.s.l.
Agriculture surface usage	367000 ha
Forests	252000 ha
Irrigated surface	20000 ha
Industrial usage	305 millions m^3/year

Table 3.2: Sub-basins of the Arno catchment

Sub-basins	**Area** (Km^2)
Casentino	895
Valdichiana	1362
Upper Valdarno	997
Sieve	846
Middle Valdarno	1375
Lower Valdarno	3641

3.1.2 River Catchment

The basin covers an area of 8228 km^2. As of February 2017, the catchment management is supervised by the Northern Apennine District Basin Authority (Autoritá di Bacino Distrettuale dellAppennino Settentrionale), implementing the application of the EU Floods Directive. The area is divided in 6 sub-basins as showed in the Tab. 3.2.

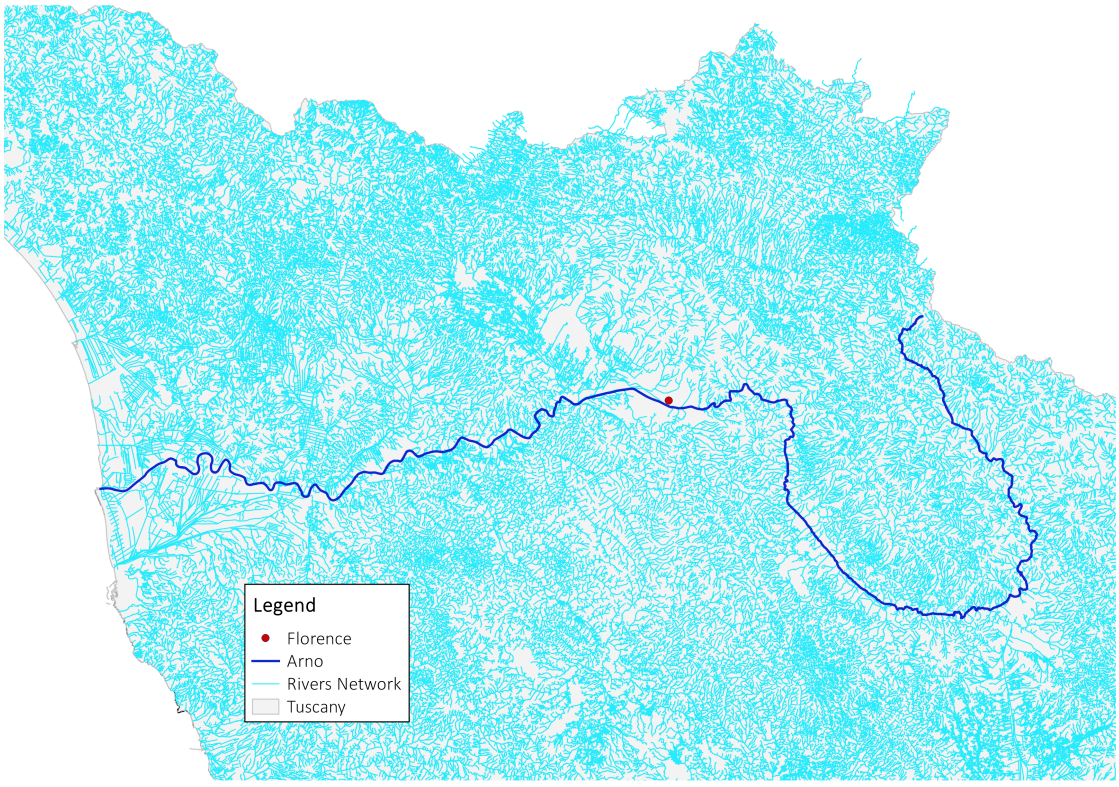

Figure 3.2: Detail of the river network in proximity of the Arno river

The rivers and streams network flowing inside the basin is very thick. The main ones are: from the left side Greve, Pesa, Elsa, Ambra, Era and from the right side Sieve, Mugnone, Bisenzio, Ombrone pistoiese.

3.1.3 River History

Besides the problems connected to the floods the Arno river has always played an important role from an historical point of view. Since the ancient times, a lot of villages and towns took advantage of its waters to grow up and develop, including Florence that reached its prosperity peak during the Renaissance. The Arno stream was navigable and represented the main route for trading and transporting goods until the railway was built in the 19^{th} century [33]. Small ships were able to use the sea current to reach Florence also in the dry periods. The business was mainly based on the trade of iron from the Elba Island as well as the trade of wood and fabric.

3.1.4 Monitoring System

The hydrological and hydraulic monitoring system is managed by Regional Hydrologic Service (SIR, Servizio Idrologico Regionale) that ensures the management of the environmental data survey network, the data survey from the recording stations and the validation of the data.
The regional survey network of the hydro-meteorological data counts more than 450 stations that include rain, height and wind gauges. The main stations regarding the Arno river are listed in Tab. 3.3.
The recording data stations mentioned above are represented in the Fig. 3.3.

Table 3.3: The main stations regarding the Arno river

Name	**Type of measurement**	**Height (m.a.s.l.)**
Stia	Discharge, Water Level	479
Subbiano	Discharge, Water Level	226
Montevarchi	Discharge, Water Level	163
Incisa	Discharge, Water Level	105
Nave di Rosano	Discharge, Water Level	80
Firenze Uffizzi	Discharge, Water Level	50
Ponte a Signa	Discharge, Water Level	38
Empoli	Discharge, Water Level	38
San Giovanni Vena	Discharge, Water Level	16
Pisa Agraria	Water Level	6
Bocca d'Arno	Water Level	1

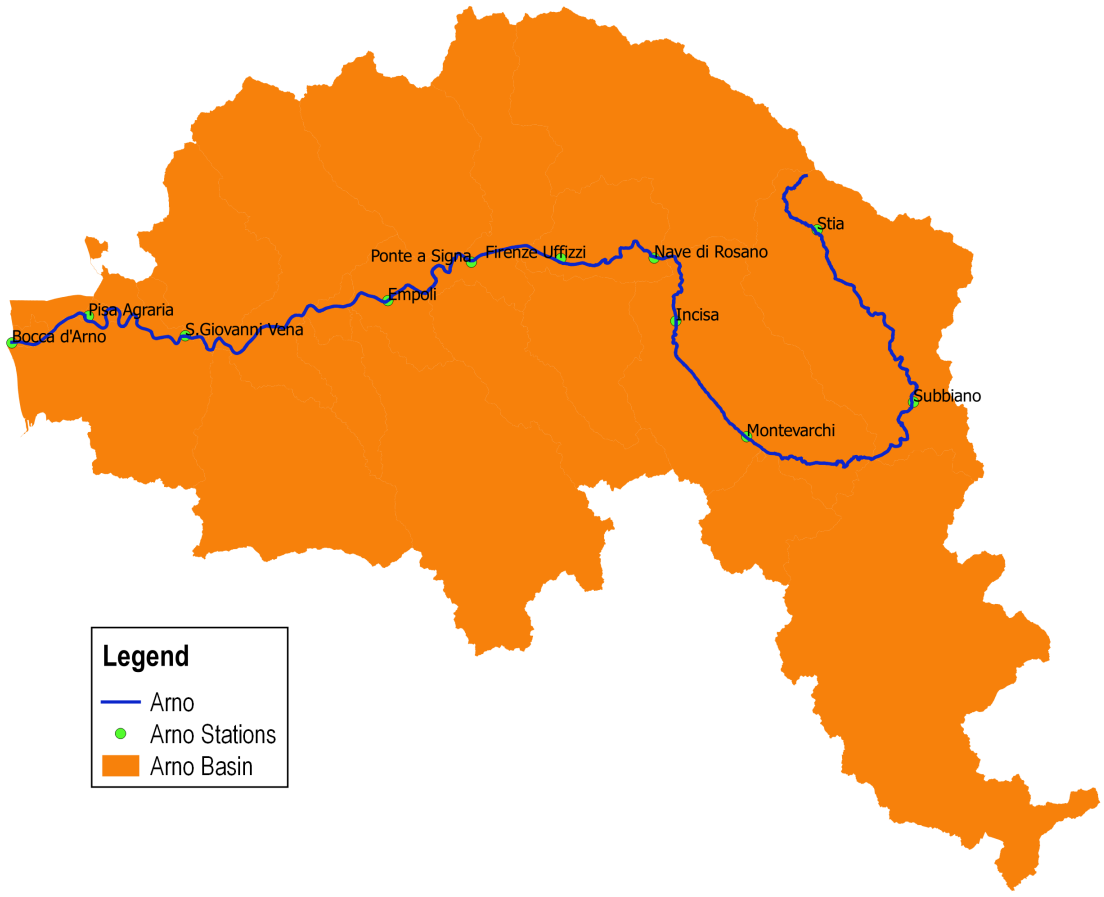

Figure 3.3: Arno basin and the main recording stations of the river

3.2 Case of Study

The case of study for the present work is focused on the Arno river that flows through the urban part of Florence. In particular, the river reach under investigation is contained between the cross section AR0585 and the cross section AR0558 covering a distance of around 1.4 Km. Within the reach considered, there are five important hydraulic structures: four bridges and one weir. From the upstream to the downstream Ponte Vecchio, Ponte Santa Trinita, Ponte alla Carraia, Pescaia di Santa Rosa and Ponte Vespucci. The structures are shown in Fig. 3.4.

Figure 3.4: Stretch of the Arno river in the urban part of Florence

Ponte Vecchio has a 100 m length and a 20 m width and it is supported by two solid sharp piers. It was built for the first time in the Romans age but has been damaged and destroyed due to the flood events over the centuries. It was only in 1345 that the bridge was erected as it appears nowadays. It has three lower arches (the first of its kind) that saved the bridge from the extreme hydraulic conditions. In fact, larger spans allowed the debris to pass through with more facility and to avoid damages to the structure. Over time, some small shops were built, at first butcheries and then jewelries. In 1565, Giorgio Vasari built the Vasarian Corridor that links Palazzo Vecchio (administrative centre of Florence) to Palazzo Pitti (abode of the Medici family). During the Second World War Ponte Vecchio was the only one spared from the explosions. In 1966, the bridge was devastated from the well-known flood event, but it did not collapse. In order to safeguard the history, the symbol and the worth of the bridge, the present work aims at understanding more in depth the hydraulic dynamics and the water behaviour that characterise the river.
Santa Trinita bridge has a 100 m length and a 10 m width. As for Ponte Vecchio, there are two robust sharp piers. The bridge was destroyed and built again over time

until it was designed by Bartolomeo Ammannati and in part by Michelangelo and finally erected in 1570. The arches have an elliptic line that gives grace and enables a larger passage for the debris, as already seen above with Ponte Vecchio. After its demolition during the Second World War, the bridge was built again as an exact copy of the original.
Alla carraia bridge is approximately 133 m long and 13 m wide. Differently than the two other bridges, the structure consists of five sharp piers and subsequently of five large spans. It was built for the first time in 1218 and was subject to several collapses over time. The name has its origin from the passage of the trading carts.
Santa Rosa weir is an oblique weir which was built around the beginning of 1200. The weir has a very important role from the hydraulic point of view. Since it is oblique, the flux lines change the direction causing a recirculation zone on the left side and a huge deposit zone on the right side. Moreover, this behaviour leads to the erosion of the left pier of Ponte Vespucci. The inclination angle is 41° starting from the right side and going inside towards the left side for a total length of 228 m. The weir is not only tilted in the plane view but also respect to the horizontal line. In fact, there is a decreasing gap of 20 cm from the left to the right side.
Vespucci bridge is the youngest bridge of the above mentioned structures, since it was built only in the 20^{th} century. It has a 163 m length and a 23 m width and is characterized by two sharp piers that divide the bridge in three long spans. Furthermore, it is strongly related with the Santa Rosa weir.

(a) *Upstream Ponte Vecchio*

(b) *Upstream Santa Trinita bridge*

(c) *Upstream alla Carraia bridge*

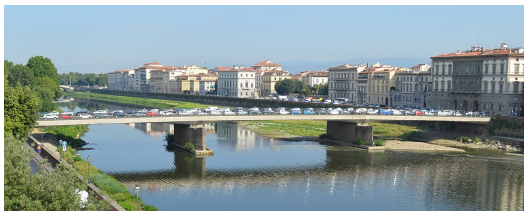

(d) *Upstream Vespucci bridge*

(e) *Downstream Santa Rosa weir*

Figure 3.5: Hydraulic structures along the river reach (source: www.wikipedia.it)

3.3 The 1966 Flood Event

On 4^{th} November, 1966 Florence was hit by an enormous flood. As mentioned in the subsection 3.1.1, flood events with a higher water discharge happened in the past, but the 1966 one was certainly the most catastrophic as regards the extension of the flooded area and the height the water reached [13]. Besides the innumerable damages to the buildings, streets, works of art and all the precious city heritage, 17 people died in the city centre. This dramatic event is still in the mind of every citizen, and the fear it could happen again is high.
The main reason causing the flood event was associated with an extreme precipitation

that ran out into the whole Arno basin. The intensity and the duration of incessant rains leaded the flood wave to hit Florence starting from 4^{th} November to 5^{th} November. As reported in [26] and based on the later studies, in those days, the alleged quantity of rain fallen in Florence would correspond to 180 mm, that is 180 liters per square meter. Even if the value recorded only in the city of Florence was very high, the extreme rain precipitation in all the rest of the basin played a fatal role. Tab. 3.4 reported the values in mm recorded by three stations placed at the beginning, in the middle and in proximity of Florence.

Table 3.4: Rain values in mm recorded in 4^{th} November 1966 in three gauges

Gauge	**Rain** (mm)
Stia	167.0
Montevarchi	179.4
Firenze Ximeniano	131.6

The main factors that concurred and had more effect on the tragic events were [26]:

- The water levels of the Arno river were already higher than the normal when the catastrophe took place because of previous rains in October.
- The soil was completely saturated because of the persistent rainfalls.
- The precipitation was particularly strong and intense.

As regards the discharges, new historical records were recorded everywhere in the basin. Fortunately, the discharge peak of the Sieve river, one of the most important tributary stream, reached Florence in delay. This extended the time of inundation but did not increase the discharge peak of the Arno river which could cause even more damages. Tab. 3.5 shows relevant values in three different positions [8].

Table 3.5: Discharge values in November 4^{th} 1966 in three gauges

Gauge	**Discharge** (m^3/s)
Stia	312
Subbiano	2250
Nave di Rosano	3540

During the night of 3^{rd} November, the water level quickly raised, one meter every hour, for six consecutive hours, until the water overtopped the levees and flooded

into the city collapsing in some points.
Fig. 3.6 and Fig. 3.7 show the reconstruction of the flood hydrographs for the main rivers of the basin and the areas interested by the event.

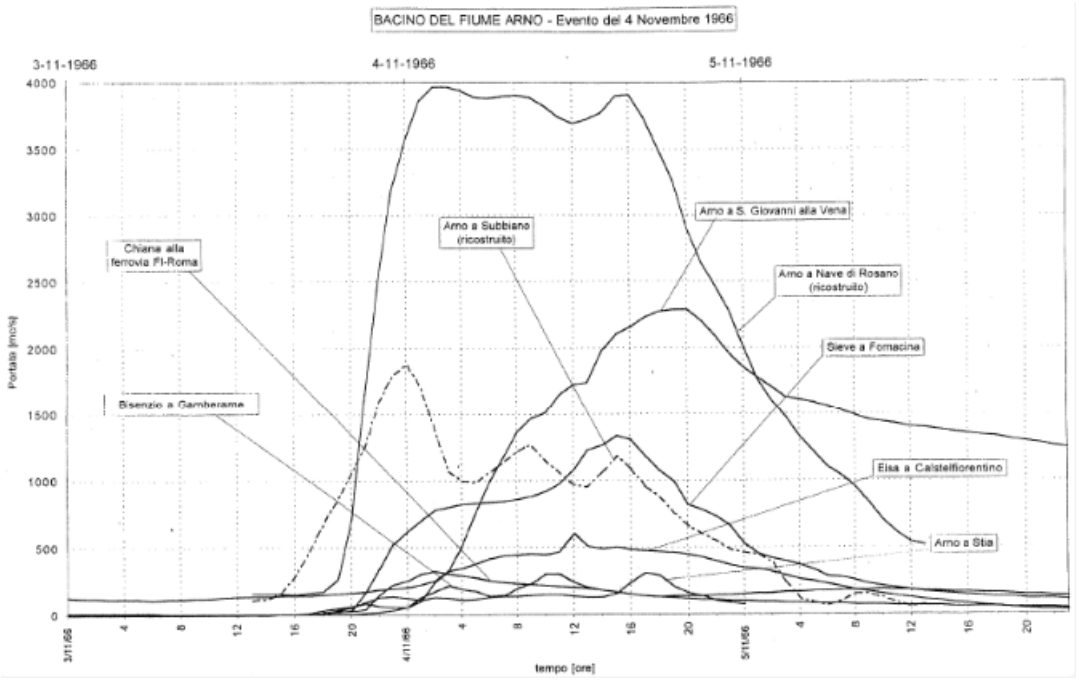

Figure 3.6: Reconstruction of the flood hydrograph of the main rivers (source: adb Arno)

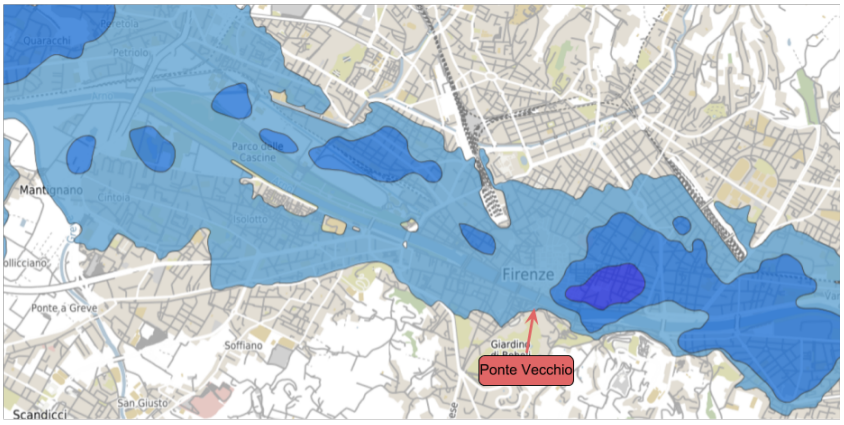

Figure 3.7: Flooded areas in Florence (source: adb Appennino Settentrionale)

During the flood event, the hydraulic structures, mentioned for the purposes of the present work, were in part or completely submerged by the water. Furthermore the

presence of the structures, in particular Ponte Vecchio and Santa Trinita bridges caused a strong backwater effect that contributed to an additional increase of the water level.
Fig. 3.8 gives an idea of the complex situation and illustrates the water level reached in proximity of the bridges.

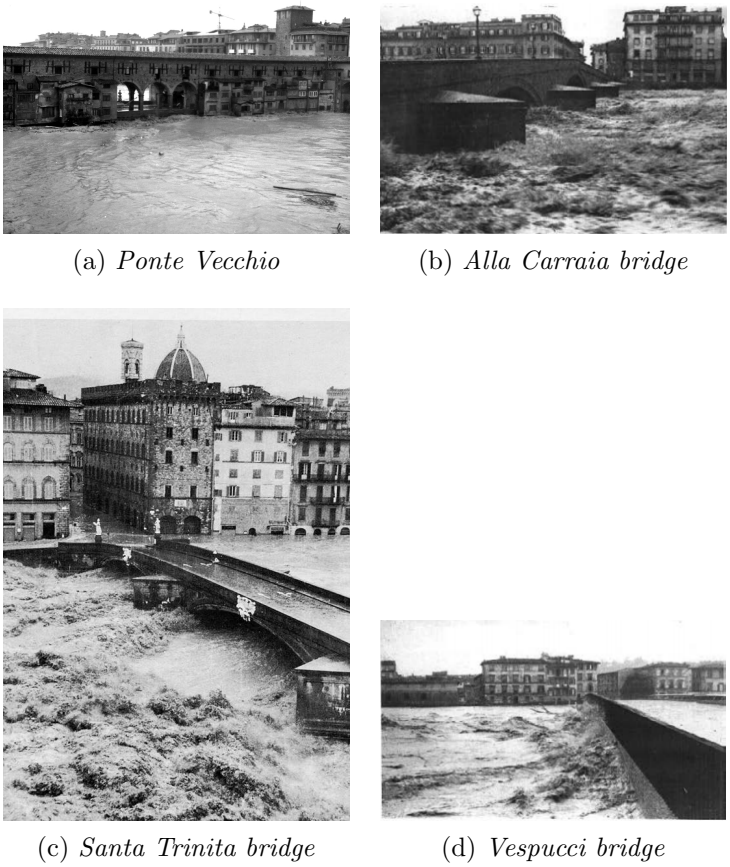

(a) *Ponte Vecchio* (b) *Alla Carraia bridge*

(c) *Santa Trinita bridge* (d) *Vespucci bridge*

Figure 3.8: Water level in proximity of the bridges (source: [13])

3.4 After 1966 and Bologna Scaled Model

During the days of November 1966 the wave of bad weather hit not only the Tuscany, but whole Italy. The dramatic events pushed Italy to react and to create a new hydro-geological arrangement in order to prevent other dangerous situations. Therefore, the *inter-ministerial Commision for the study of the hydraulic solution and the soil defence*, called De Marchi Commision (from the name of the President), was established. The management of the several geographical areas was assigned to sub-commissions with the purpose of identifying defence strategies against flood events [10].

The sub-commission in charge to deal with the Arno river basin was managed by Professor Giulio Supino, and the actions provided for reducing the hydraulic risk of the Arno river were collected in the so called *Supino Plan*. The plan was focused on the realisation of the detention basins for the Arno river and its main tributary streams. This detention basins amounted to 23 reservoirs of which 17 were upstream and 6 downstream of the city of Florence.
In this context, in 1972, the *Genio Civile* of Florence commissioned the University of Bologna to create a scaled model of the Arno river in proximity of the urban reach of Florence. More exactly from Alle Grazie bridge to the Santa Rosa weir. Since the indirect actions were focused on the creation of detention basins, the Bologna project was tasked to work on direct actions on the river. The idea was to lower the slabs of Ponte Vecchio and Santa Trinita bridge. As described in the final report [11], the objectives were:

- Analysing the free surface behaviour in the current hydraulic condition without the slab modification and with various discharges close to the maximum.
- Establishing the overflowing in the current hydraulic condition without the slab modification caused by the maximum discharge.
- Identifying the maximum discharge contained in the river with the slab modification.

(a) *Ponte Vecchio Upstream*

(b) *Alla Carraia bridge*

(c) *Santa Trinita bridge*

(d) *Overall overview*

Figure 3.9: Pictures of the model (source: [11])

The experimental model was built in scale 1:60. The stream is included between two masonry walls. The water is activated from an upstream tank and collected from a second downstream tank. The bridges were built of wood painted with waterproof material. The weir was built in masonry like all the slabs of the bridges. On the base of a field survey the material chosen for the bottom is gravel of the size of 8 mm, corresponding to a Manning's roughness value of 0.0435 [13]. A fixed bed was supposed. The measurement of the free surface was carried out with a pointed gauge while for the water discharge a calibrated nozzle was used. Five tests were measured:

- 1^{st} case: considering the current situation.

- 2^{nd} case: lowering only the Ponte Vecchio slab of 1 m.
- 3^{rd} case: lowering both the slabs of Ponte Vecchio and Santa Trinita bridge of 1 m.
- 4^{th} case: lowering only the Santa Trinita bridge slab of 1 m.
- 5^{th} case: lowering both the bridges as in the 3^{rd} test, but with an inverted arch configuration.

The results can be summarised as following:

- The lowering of only the Ponte Vecchio slab was negligible since the benefits in terms of discharge contained in the river were not sufficient.
- The lowering of the slabs of both the bridges (3^{rd} test) implied more advantages. The maximum discharge contained in the river banks was increased respect to the situation without modifications. The increase went from 3090 to 3450 m^3/s.
- In the case of a 3000 m^3/s discharge, the backwater effect in proximity of Ponte Vecchio and Santa Trinita bridge was significantly reduced.

Tab. 3.6 shows a comparison of the hydrometric levels for a discarge of 3000 m^3/s for Ponte Vecchio, Santa Trinita and Alla Carraia bridges, applied to the simulation models without and with both the slab modifications.

Table 3.6: Comparison for a discharge of 3000 m^3/s

Bridge	Water Level (m) No slab modifications	Water Level (m) Both slab modifications
Ponte Vecchio upstream	48.94	48.11
Ponte Vecchio downstream	48.53	47.59
Santa Trinita upstream	47.96	47.53
Santa Trinita downstream	47.67	46.83
Alla Carraia upstream	46.72	46.65
Alla Carraia downstream	46.10	46.04

Tab. 3.7 shows a comparison of the hydrometric levels for the maximum discharge contained in the river (3000 m^3/s and 3450 m^3/s) for Ponte Vecchio, Santa Trinita and Alla Carraia bridges to the simulation models without and with both the slab modifications. The construction of the two slabs started in 1977 and finished in 1980.

Table 3.7: Comparison for the maximum discharge

Bridge	Water Level (m) No slab modifications	Water Level (m) Both slab modifications
Ponte Vecchio upstream	49.20	48.97
Ponte Vecchio downstream	48.84	48.61
Santa Trinita upstream	48.28	48.12
Santa Trinita downstream	47.92	47.55
Alla Carraia upstream	46.99	47.26
Alla Carraia downstream	46.25	46.72

3.5 Data and Preliminary Processing

The following section has the purpose to give more details about the data and the preliminary phase preceding the model simulation. This part has a particular relevance for the achievement of the fixed objectives. In fact, the following data represent the base on which the model is built and from which the results depend.
The data included in the present work have been collected by the Civil and Environmental Engineering Department of the University of Florence between 2014 and 2016.
The monitoring system was composed by three activities [25]:

- A three-dimensional survey of the Arno river bed with the aim of representing more in details the conditions of the channel, in particular the deposit and the erosion zones;
- Measurements of the flow and the sediment discharges;
- Sediment survey with the objective of defining the grain size curve.

All the mentioned activities result in the creation of a physically based hydraulic model of the Arno river. However, only the first two field data are used for the present work.

Figure 3.10: Phases of the survey (source: [25])

3.5.1 Topography Data

In recent years, the cross section method was used to collect information on the Arno river topography. The measurements could be collected only along the transverse line of the survey. Hence the bottom between two sections is unknown. The reach of the urban part of Florence is characterised by a high number of hydraulic structures which have a relevant impact on the river dynamic, in particular regarding local phenomena. Therefore, the cross section method is not sufficiently adequate to collect accurate information.
In order to learn the precise river topography, the three-dimensional survey was carried out through an appropriate boat. Two technologies were used:

- Multi Beam Eco Sounding (MBES) technology for the river bed, consisting of measurements under the water through an echo-sounder. The navigation on the river is managed through GPS. Sensors for the equalization of the boat movements were used to increase the accuracy of the tools.

- LIght Detection And Ranging (LIDAR) technology consisting of a laser scanning for the emerged part.

The data collected through the survey created two point clouds, one for the bed of the river and one for the emerged structures. The two technologies allowed the Engineering Department to obtain the Digital Terrain Model (DTM).
The investigation of the river was realised on an 18 km reach, from Varlungo to Ponte a Signa. On the basis of navigation issues and morphological limits, seven sections could be distinguished:

- Zone 1: from Varlungo viaduct to San Niccoló weir.

- Zone 2: from San Niccoló to alle Grazie bridge.

- Zone 3: from alle Grazie bridge to Santa Rosa weir
- Zone 4: from Santa Rosa weir to Isolotto weir
- Zone 5: from Isolotto weir to Indiano viaduct
- Zone 6: from Indiano viaduct to Greve outlet
- Zone 7: from Greve outlet to Ponte a Signa

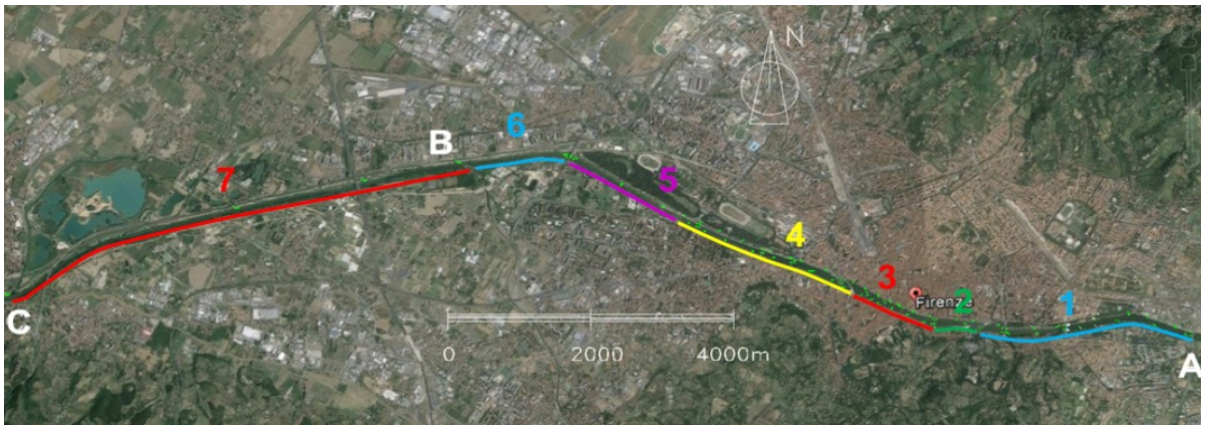

Figure 3.11: Sections of the survey (source: [25])

The distribution of the detected points is not uniform: a higher number of points was measured in the areas (urban reach) where a higher accuracy was requested. In the peripheral part, where the banks were covered by vegetation, a larger cloud was favoured.
In order to reduce the discrepancy between the estimated and the actual positions of the points, 80 Ground Control Points (GCP) were used. In this case the GCP were represented by A4 papers installed in several key spots and detected during the survey, which were further elaborated to adjust and correct the position of the clouds.

Topography Setting

As described in the previous paragraph, the points have been collected with two different techniques: MBES for the river bed and LIDAR for the emerged structures, which includes banks and bridges. As said, they represent two different clouds. In order to exploit the field measurements for the present work, the rough data has been further elaborated for the creation of the channel where the river flows through in the simulation. Hence, the river bed and the banks points have to be part of the same cloud. The bridges have been removed using the software *Autocad 2018*. Then,

the data have been cleaned from the non-significant points and finally merged in one cloud. The topography for the channel is now ready to be used both for CFD and SFLOW simulation.
The structures, like bridges and weirs, represent one of the main aspects since they have important effects on the river hydraulics. For this reason their design has to be as detailed as possible. The Engineering Department of the University of Florence provided the *.dwg* file including the bridges and the weir related to the river reach under investigation. The structures have been elaborated again for the present work and introduced in the CFD model through a *.stl* file.

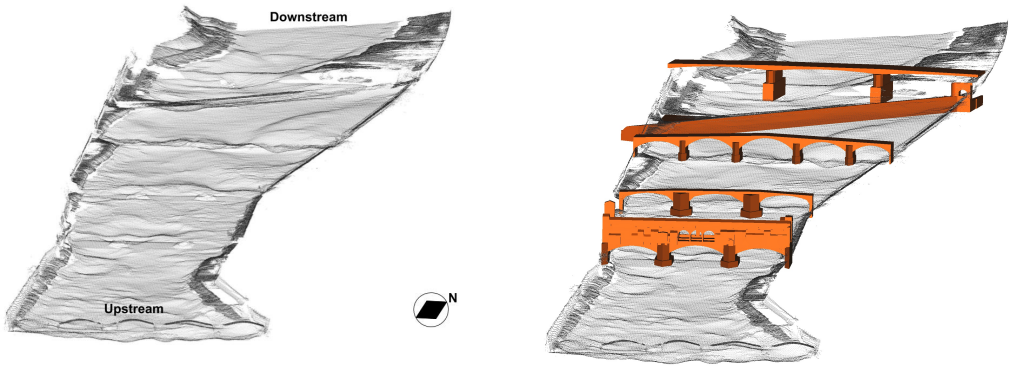

(a) *River bed and banks* (b) *River bed, banks and structures*

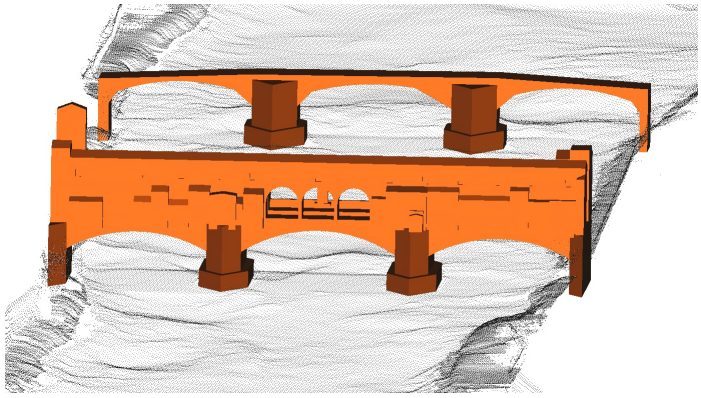

(c) *Details of Ponte Vecchio and Santa Trinita bridge*

Figure 3.12: Setting of the topography.

Nevertheless, in the SFLOW model, the structures cannot be represented through the *.stl* file. Since it is a two-dimensional model, the grid mesh can affect the solids during the simulation. In particular, the cells along the vertical axis can be positioned in a wrong way. The issue can be solved by replacing the whole structures with only the piers of the bridges. A qualitative framework of the river hydraulics is preferred within this approach.

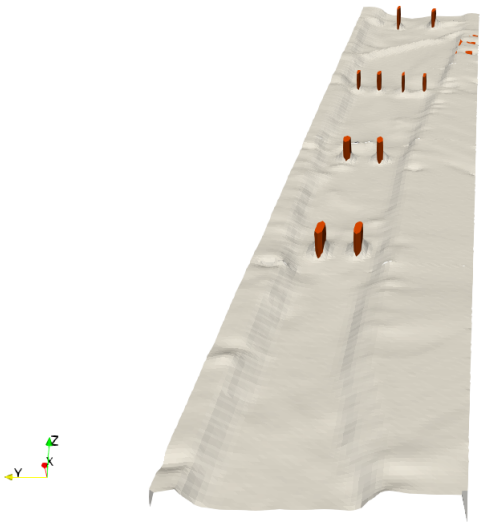

Figure 3.13: Bridge piers created for the SFLOW model

Boundary Conditions

Also, it is worth mentioning that the boundary conditions are very important elements for the results of the simulations. Since they can have a high influence on the model, a particular attention is needed during the setup.
Every model needs two conditions:

- inflow boundary condition;
- outflow boundary condition.

As regards the inflow, a constant discharge is defined. Part of the discharge values from the field survey and from previous Bologna experiments are used.
At the outflow, a specific water level is set. The Civil and Environmental Engineering Department of the University of Florence made additional data available from a mono-dimensional simulation using the *Hec-Ras* software. The Hec-Ras simulation provides the water levels for several discharge values for each cross section represented in the model.

3.5.2 Discharge Measurements

The mathematical model represents an important instrument to evaluate the hydraulic risk. In this context, the field measurements are needed since the discharge

values allow the model to be calibrated and validated.
For the present case study, it is considered the discharge measurement station located on Alle Grazie bridge around 500 m before Ponte Vecchio. Along the bridge nine spots detected the values through specific tools to evaluate the instantaneous velocity and the water level. After laboratory analyses, the discharges have been acquired.
The data have been collected in three different time periods:

- between January and February 2014 during the flood period;
- between July and October 2015 during the low water period;
- between January and February 2016 during the flood period.

The most complete and available set of data is represented by the last survey collected in 2016. Tab. 3.8 summarises the discharge measurements and the respective water levels of the Ponte Vecchio, Santa Trinita, Alla Carraia and Vespucci bridges. The water levels are referred to the centre line of the bridges.

Table 3.8: Discharges and water levels for each bridge. Note: water levels represent the height with respect to the sea level.

Bridge	**Discharges**				
	9.5 (m^3/s)	**63.8** (m^3/s)	**250** (m^3/s)	**321** (m^3/s)	**909** (m^3/s)
	Water Level (m a.s.l.)				
Ponte Vecchio upstream	41.44	41.73	42.09	42.33	43.43
Ponte Vecchio downstream	41.45	41.71	42.06	42.29	43.52
Santa Trinita upstream	41.41	41.67	42.07	42.26	43.16
Santa Trinita downstream	41.34	41.72	42.04	42.24	43.10
Alla Carraia upstream	41.39	41.61	42.00	42.15	42.98
Alla Carraia downstream	41.36	41.68	42.01	42.14	42.86
Vespucci upstream	36.43	36.89	37.59	37.95	39.64
Vespucci downstream	36.33	36.72	37.62	37.86	39.61

Tab. 3.8 is used for the hydraulic model validation. Since the data have been collected during direct field surveys, the discharge values are quite low. In order to have an idea of the possible scenario subsequent to flood events, higher discharges are used for the present work. Specifically, it has been decided to use the same values of the Bologna experiments in order to have comparable water levels for the validation of the model.

Chapter 4

Results

Before moving forward with the results of the study case, a brief description of the passages needed for the achievement of the objectives will be discussed below. First, the validation of the software will be performed through the analysis of two cases in relation to a weir and a double pier. This part is very important to test the reliability of the program. Since the hydraulic model needs to be created gradually, the cases analysed will shift from simple to more complex situations. For this reason, the double pier case will be used both for the validation and for the first step of the model development. In fact, it is composed by a non-complex structure (the piers) and a non-complex bottom (a flat river bed without topography). The next step includes the analysis of the arch bridge case that follows the validation section. It is composed by a complex structure (the arch bridge) and still a non-complex bottom. This case can be considered quite interesting for the physics of the scenario, since the shape of the bridge is similar to the old bridges in Europe, dating back to the Roman and the medieval times. The similarities with Ponte Vecchio represent an important motivation for the study of the arch bridge. The last step describes the Arno river case. The complex hydraulic structures and the topography for the river bed together with the discharge data represent the most complex case and a hard challenge for the success of the model simulation.

4.1 Validation

In the context of the software validation, two specific situations are analysed and compared with experimental data: flow around a double pier and over a weir.
In the channel flow, the free surface motion is one of the main characteristics to consider. It is strictly related to the river morphology and to the presence of hydraulic structures. In case of narrow passages or bridge piers, the cross section, in which the water flows through, is reduced and influences the natural free surface behaviour.

As expressed by the Bernoulli's equation, the total energy of the the flow remains constant. Therefore, if the section is reduced, the flow velocity increases to balance the equation. In the context of hydraulic changes along the channel, the flow regime could quickly pass from sub-critical to super-critical or vice versa, depending on the situations.
One of the most important parameters that governs the river is the *Froude Number* Fr. It is defined as follows:

$$Fr = \frac{U}{\sqrt{gy}} \tag{4.1}$$

where U is the average velocity, g the gravity and y the water depth.
If $Fr > 1$, the regime flow is *super-critical*.
If $Fr = 1$, the regime flow is *critical*.
If $Fr < 1$, the regime flow is *sub-critical*.
Also, the *specific energy* E and the *critical depth* y_{cr} are purely related to Fr as shown in the Fig.4.1.

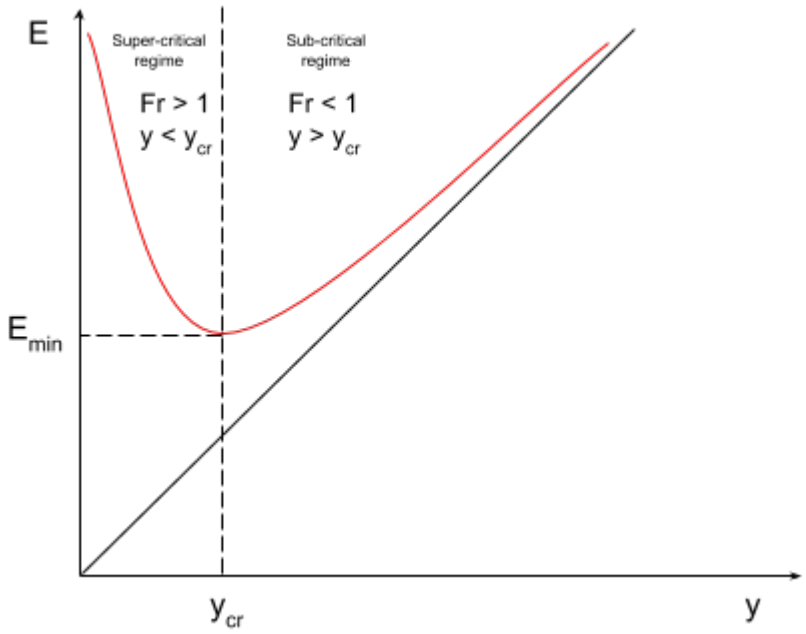

Figure 4.1: Super and sub-critical regimes scheme.

The minimum of the specific energy along the vertical axis corresponds to the critical depth along the horizontal axis. This point delimits the super and the sub-critical regimes. Furthermore, when the water depth is in proximity of y_{cr}, the water discharge flows through the section with the minimum of the specific energy.

4.1.1 Flow around a double pier

This case considers the flow around two piers as in the experiments by Szydlowski (2011). As shown in Fig. 4.2, the channel is 4 m long and 0.622 m wide. Both piers are placed 1.3 m downstream of the inflow with a 0.11 m diameter. The distance between the walls and the piers is constant and equal to 0.134 m. For the outflow, a 0.19 m water level is fixed while for the inflow a 0.114 m^3/s discharge is used. The purpose of the simulation is to check the free surface behaviour along the whole domain. For this reason, the focus of the investigation is on the water depths along the centre of the channel (0.31 m) and on a pier on the centre line (0.19 m). A grid convergence study (presented in Fig. 4.3) involves three different grid sizes dx: 0.01 m, 0.025 m and 0.05 m. The results have converged from a grid size of dx=0.01 m. This cell size has been chosen to compare the simulation results with the experimental data.

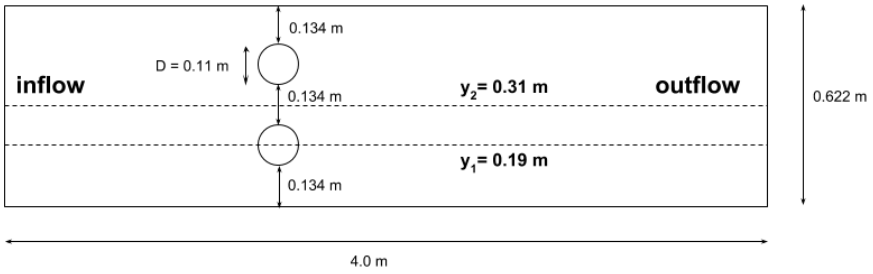

Figure 4.2: Numerical setup of the double pier model.

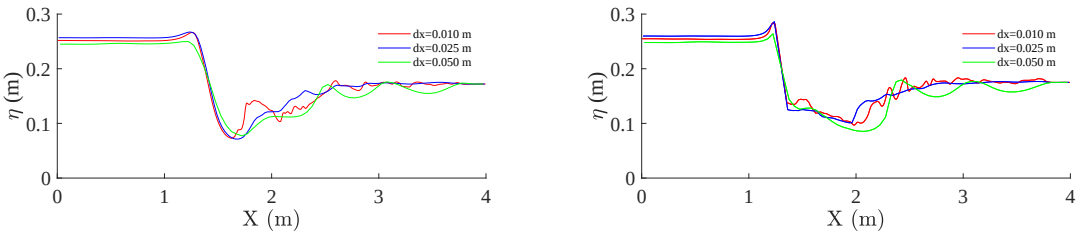

(a) *along the centre of the channel (0.31 m)* (b) *along the centre of the pier (0.19 m)*

Figure 4.3: Grid convergences study for the free surface line for the double pier case.

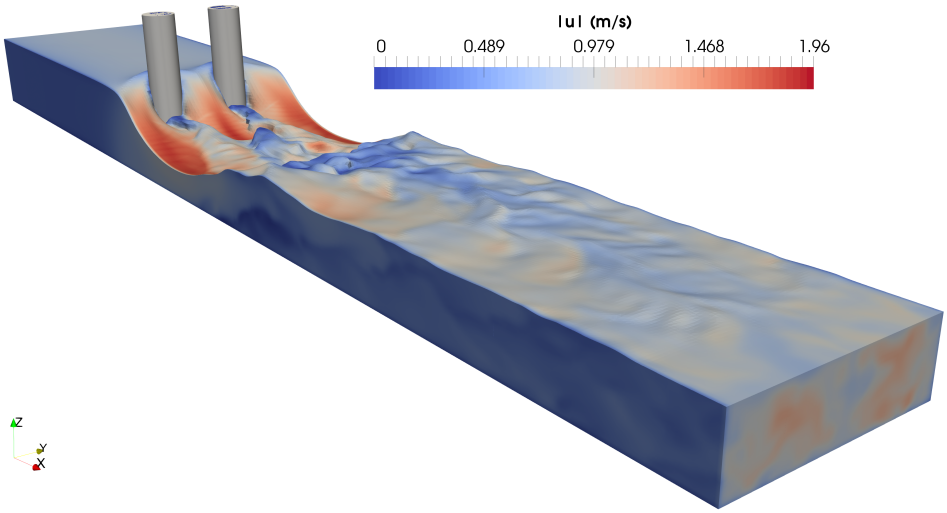

Figure 4.4: Free surface with velocity magnitude contours for the double pier case.

Fig. 4.4 shows the free surface features with the velocity magnitude contours. The flow regime starts from a sub-critical condition. During the passage through the piers, it then changes to super-critical and goes back again to sub-critical. In order to pass through the piers, the flow has to accelerate and then to slow down when the section widens. In the last phase, higher energy losses are registered. Considering the hydrodynamics theory, the free surface is represented with two different profiles *M2* and *S2* linked together by an hydraulic jump.
The numerical results from the simulation well-represents the experimental data for both the middle of the channel and along the centre line through the pier as shown in Fig. 4.5. The graphs represent the free surface levels over the space. Also the super-critical part is simulated reflecting the experiment with a good matching of the points.

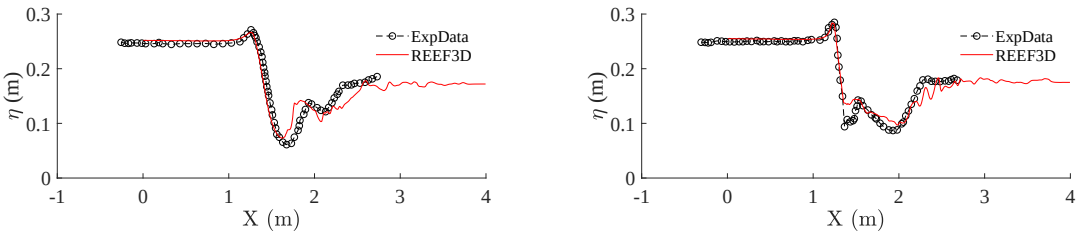

(a) *along the centre of the channel (0.31 m)* (b) *along the centre of the pier (0.19 m)*

Figure 4.5: Comparison of the free surface levels between the results of the simulation and the experimental data (Szydlowski 2011).

For the sake of completeness, the velocity profiles in various specific spots are represented in Fig. 4.6. More exactly, the profiles are extrapolated for x = 0.6 m, 1.3 m, 1.7 m and 2.6 m. The 1.7 m profile is particularly interesting because it is placed in proximity of the hydraulic jump, when the regime is super-critical. In this section, the water depth is the lowest and the velocity along the x-direction is maximum.

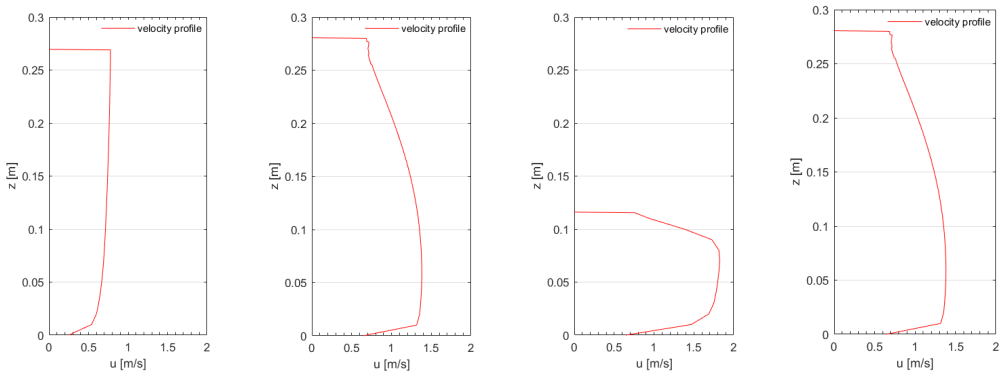

(a) $x = 0.6\ m$ (b) $x = 1.3\ m$ (c) $x = 1.7\ m$ (d) $x = 2.6\ m$

Figure 4.6: Velocity profiles along the x-direction in various spots of the channel.

Furthermore, as mentioned above, this case can be considered the first step for the creation of a more complex model as the Arno river because of the presence of a flat river bottom and the simplicity of the hydraulic structures.

4.1.2 Flow around a 3D weir

This case considers the flow over a rectangular broad-crested weir as in the experiments by Sarker and Rhodes (2004). The numerical setup of the model is shown in Fig. 4.7. The channel is 3.16 m long and 0.105 m wide. The weir is placed 1.2 m downstream the inflow and it is long 0.4 m. The initial water level is set to 0.19 m. For the inlet, a 0.004684 m^3/s discharge is used while for the outlet, a free stream outflow is fixed. The free surface behaviour is analysed along the centre of the channel. Also for the broad-crested weir, a convergence study (presented in Fig. 4.8) involves three different grid sizes dx: 0.005 m, 0.01 m and 0.025 m. The convergence is achieved using a grid size of dx=0.005 m.

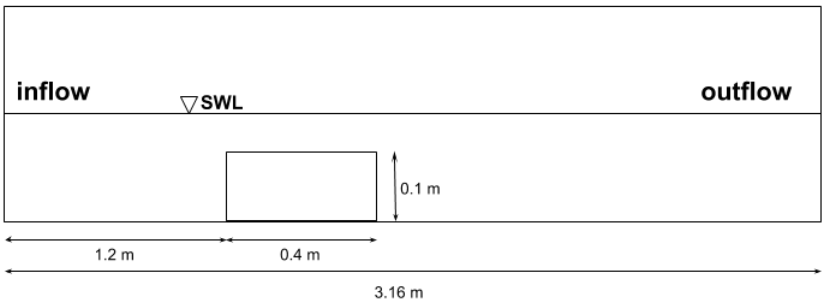

Figure 4.7: Numerical setup of the model.

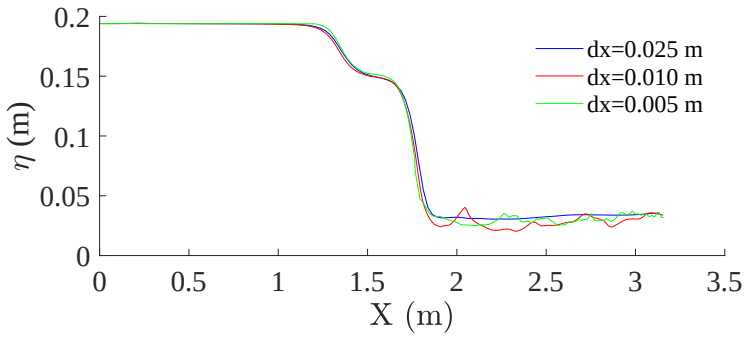

Figure 4.8: Grid convergences study for the free surface line for the broad-crested weir case.

The free surface features are shown in Fig. 4.9. At the beginning, the regime of the flow is sub-critical and then changes to super-critical passing through the weir and until the end of the domain. Furthermore, the presence of the hydraulic structure has effects on the free surface also after passing the weir.
The numerical results from the simulation are a good representation of the experimental data. The graph, represented in Fig. 4.10, displays the surface levels over the space for both data sets. It can be noticed a good correspondence of the points.

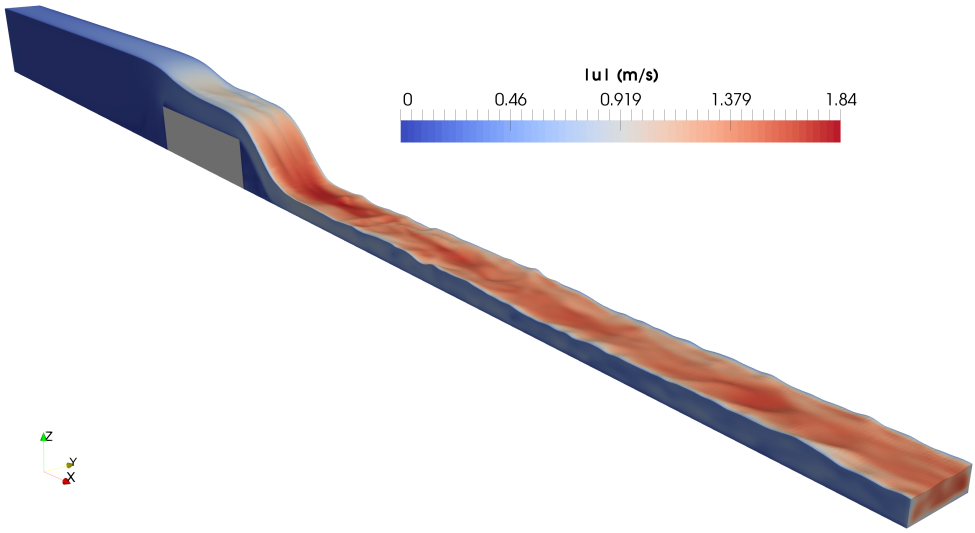

Figure 4.9: Free surface with velocity magnitude contours for the weir case.

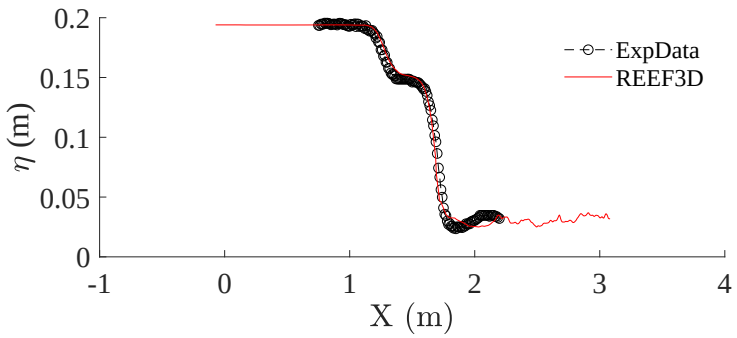

Figure 4.10: Comparison of the free surface levels between the results of the simulation and the experimental data (Sarker and Rhodes 2004).

4.2 Flow around an arch bridge

Sub-critical flow

This case considers the flow through an arch bridge using the experiments by Martin-Vide and Prio (2005) [23]. In particular, the research was focused on the backwater effects in semicircular arch bridges under free and submerged conditions. The hydraulic structure used for the research represents a complex shape that has effects on the water flow. Assuming a flat bottom, this case can be considered as the middle step for the creation of the Arno river cases. Moreover, the shape of the bridge is inspired to the Roman and to the medieval times. Since some of the Florence bridges

along the Arno river were built in that period (including Ponte Vecchio), this case is interesting for the objective of the present work. Another essential aspect is represented by the study of the water behaviour in a submerged condition, an unknown situation that can take place during extreme flood events.

The tests have been conducted on an horizontal flume: 4.5 m long, 1.48 m wide and 0.48 m high with a fixed bed. The bridge is placed 1.8 m downstream of the inflow with a length of 0.4 m and with a width of 1.48 m. Along its width, 4 arches are equally spaced with a 0.25 m span each. The three central piers are 0.12 m wide, while both the side piers measure exactly half of the central ones. The shape of the arches is semicircular with a 0.125 m radius. In the original experiments by Martin-Vide and Prio, the bridge was provided with a mechanical device that allowed the bridge to move up and down along the vertical axis. In order to reach the research purpose (analysing the backwater effects in semicircular arch bridges under free and submerged conditions), several series of experiments were conducted. For each series the discharge Q and the water level y were kept constant while the bridge was lowered. The lowering impacts the flow conditions changing them from free surface to pressurised. For this work, only one of the series has been chosen in order to validate the simulations. The selected series has a higher Froude Number Fr than the others in order to make the current effects clearer. A very important aspect regards the flow regime: in the experimental series, it was always subcritical, that means $Fr < 1$. The flume numerical setup and some details of the bridge are shown in Fig. 4.11 and Fig. 4.12 respectively. The main hydrodynamic values of the series are described in Tab. 4.1. Moreover, the flume symmetry makes it possible to consider only one span to record the backwater results and the water surface levels. To this aim, it has been chosen a parallel line to the x-axis passing through the centre of one of the central spans.

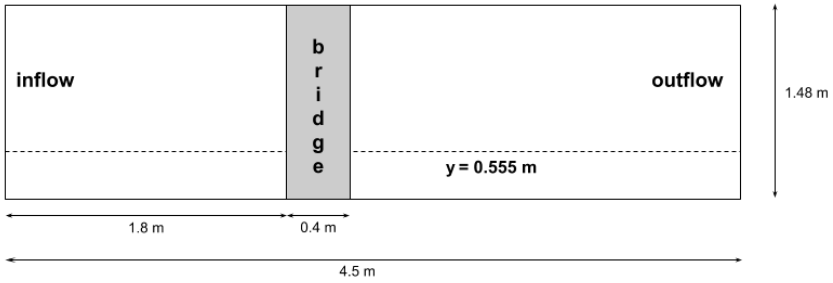

Figure 4.11: Numerical setup of the arch bridge model.

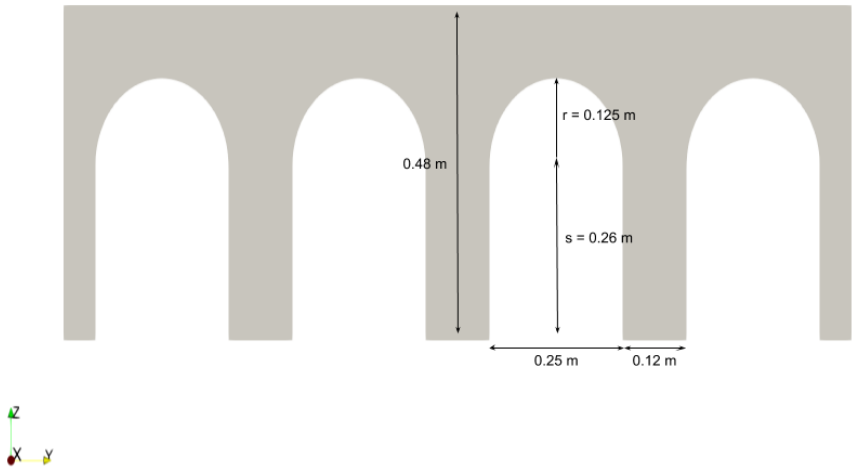

Figure 4.12: Bridge dimensions in the arch bridge model: r is the arch radius and s is the abutment elevation with respect to channel bottom related to the s=26 cm abutment.

Table 4.1: Experiment values for the C series

Series	**Q** (m^3/s)	**y** (m)	**Bed**	**Fr** $(-)$
C	0.1243	0.198	Fixed	0.300

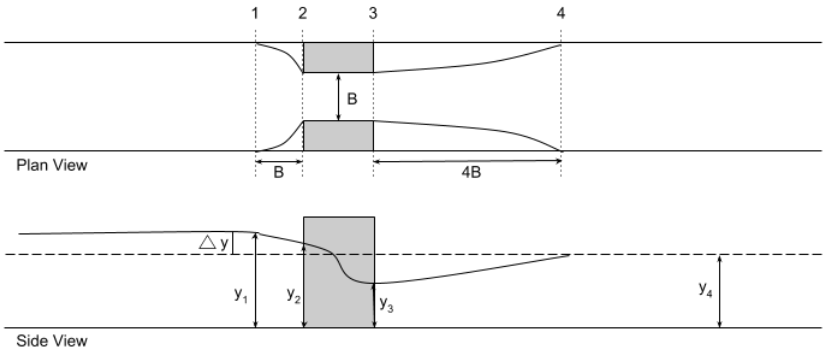

Figure 4.13: Plan and Side views related to the bridge backwater theoretical approach.

The theoretical approach is very important to understand the numerical results. Fig. 4.13 helps to make it clearer. In particular, there are four main sections:

- Section 1 is located at a span distance B upstream the bridge. In this point, the flow velocity increases due to the narrowing and the water level is specified as y_1.

- Section 2 corresponds to the bridge upstream and y_2 is the water level.
- Section 3 corresponds to the bridge downstream and y_3 is the water level.
- Section 4 is located at a four times span distance 4B downstream the bridge. This point corresponds to the tailwater. Here the bridge does not influence any longer the hydraulic conditions and the water level is specified as y_4.

The backwater elevation Δy is defined as the difference between the water elevations in section 1 and 4:

$$\Delta y = y_1 - y_4 \tag{4.2}$$

In hydraulics, the water elevations in two random sections can be computed through Bernoulli's equation. For a horizontal bottom:

$$y_1 + \alpha_1 \frac{v_1^2}{2g} = y_2 + \alpha_2 \frac{v_2^2}{2g} + \Delta H + \lambda \frac{V^2}{2g} \tag{4.3}$$

where ΔH and $\lambda V^2/2g$ express the friction loss and the local head loss across the bridge respectively.

Before simulating the tests, a grid convergence study has been conducted to make sure the best matching of the simulation results with the experimental data. The grid sizes dx involved are 0.03 m, 0.025 m and 0.01 m. Fig. 4.14 shows the backwater levels for the initial bridge abutment s=26 cm for the three cell sizes compared to the experimental value. The results converged from a grid size of dx=0.01 m. This cell size has been chosen for the simulations.

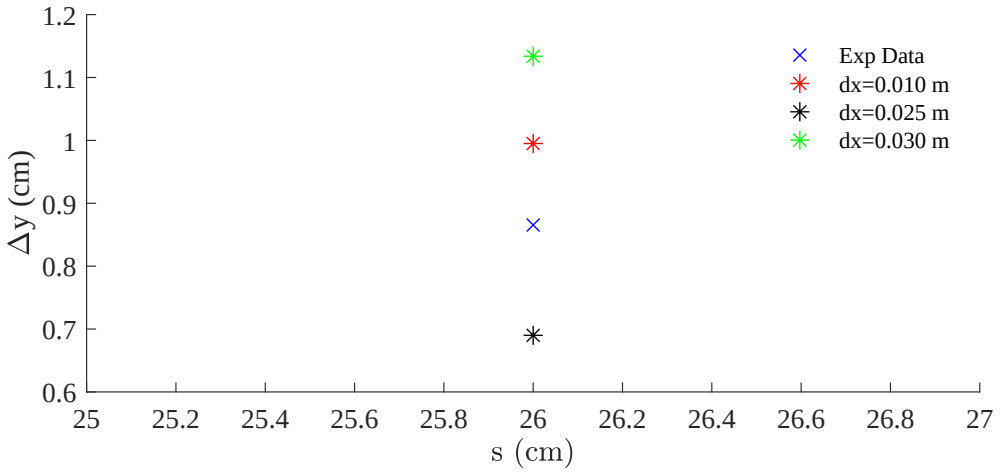

Figure 4.14: Grid convergences study for the arch bridge case.

Table 4.2: Backwater elevation values about the convergence study for abutment s=26 cm.

	dx m	**s** (cm)	Δ **y** (cm)
REEF3D	0.030	26	1.134
	0.025	26	0.690
	0.010	26	0.995
Exp Data	/	26	**0.865**

For the series C, the original experiment considered 25 tests, each one corresponding to a different bridge abutment s. Hence, 25 backwater values were available for each lowering of the bridge. For the arch bridge case, only 9 tests have been simulated, obtaining the same number of backwater levels for the comparison. In particular, the tests have been selected in order to have both free surface and pressurised flow situations: 4 and 5 respectively. Fig. 4.15 shows the free surface features with the velocity magnitude contours. Moreover, from the figure, the flow appears sub-critical as in the experiments. In order to be sure about the regime condition, an estimated Fr has been calculated. From the simulation outputs, it has been possible to define the velocity v in proximity of the tailwater when the hydraulic structure does not affect anymore the free surface. Considering the fixed water depth y=0.198 m from the experiments, Fr is given by:

$$Fr = \frac{v}{\sqrt{gy}} = \frac{0.5}{\sqrt{9.81 \cdot 0.198}} = 0.359 \tag{4.4}$$

The Fr obtained from the results matches well the Fr determined from the experiment.
Tab. 4.3 and Fig. 4.16 express the comparison between the results and the experimental data from a digital and a graphical point of view.

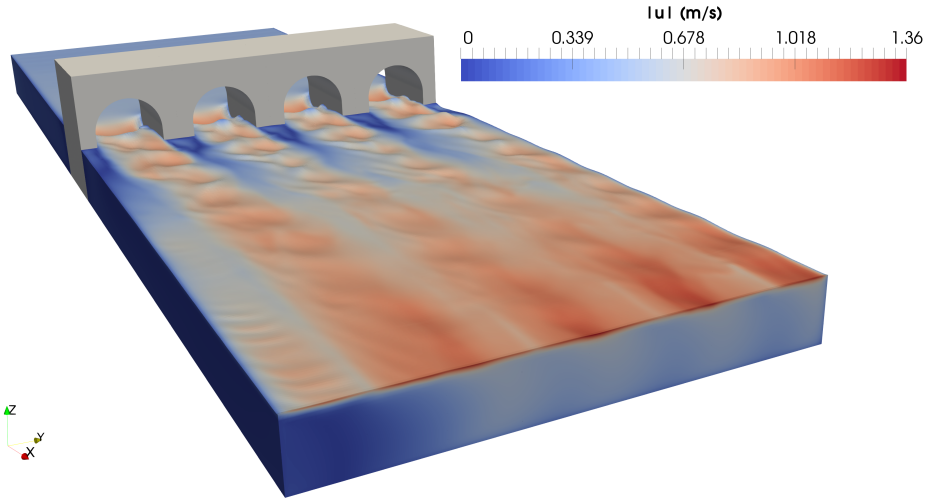

Figure 4.15: Free surface with velocity magnitude contours for the arch bridge case with an s=26 cm abutment .

Table 4.3: Experimental Data and REEF3D backwater values.

s	**Exp Data** $\Delta y(cm)$	**REEF3D** $\Delta y(cm)$
26	0.87	1.01
21	0.83	1.64
17	0.75	1.98
13	0.74	1.96
7	1.67	3.15
5	2.52	4.24
4	3.49	5.23
3	4.18	6.1
2	5.34	6.91

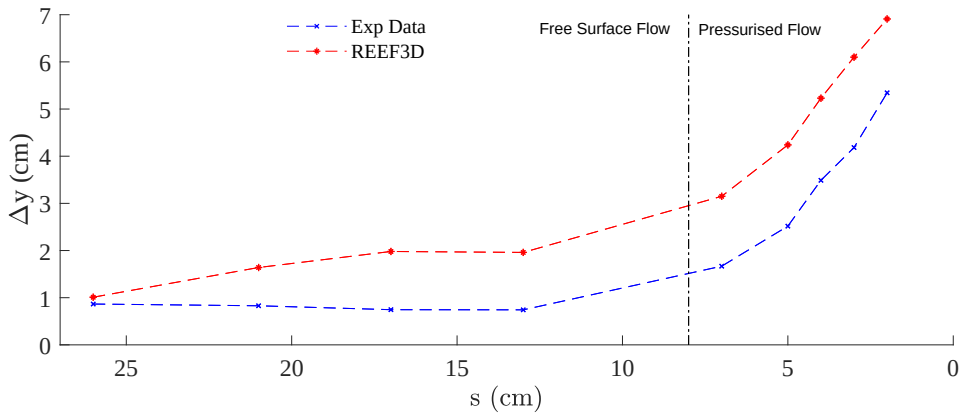

Figure 4.16: Exp Data and REEF3D backwater levels comparison.

As shown in Fig. 4.16, the vertical borderline is fixed for s=8 cm, which divides the left side of the figure representing the free surface flow from the right side representing the pressurised flow. Hence, the bridge lowers from left to right. It is important to keep in mind that a flow is pressurised when both the upstream and the downstream bridge faces are submerged. The graph displays REEF3D and the experimental data locations through points. The two starting points are very close, then a gap is kept quite constant for the other measurements. The minimum distance between the 9 measurements is recorded for s=26 cm with a discrepancy of 0.14 cm. The maximum distance is recorded for s=3 cm with a discrepancy of 1.92 cm. Even if the results are not fully corresponding, the gap is reasonable. The reliability of the results is also testified by both trend lines: their behaviour is very similar and as s decreases (the bridge lowers) Δy increases (the backwater elevation increases).

Another important aspect, that characterises the flow affected by the presence of obstacles (as the bridge piers), is the *obstruction ratio m*. It measures the severity of the constriction and it is tightly related with the complementary *opening ratio M*. As reported by Hamill in [15]: *"the smaller the opening, the greater the obstacle to flow, the greater the afflux, and the smaller the discharge through the opening"*. For this reason, m could be the main variable in the channel flow. The obstruction ratio m is defined by the following expression:

$$m = \frac{a}{A} \tag{4.5}$$

where a is the bridge face area and A is the channel area. As the bridge is composed by 4 spans, which are equally distributed for the entire width of the channel, it is possible to consider only one arch. The numerical correlation will be exactly the same. Fig. 4.17 highlights three different situations among the 9 tests simulated:

s=26 cm, s=13 cm and s=5 cm. From left to right, the water level does not cover, cover only in part and completely cover the bridge arches. This leads to different configurations. As shown in the figure, the area inside the red perimeter represents A and the hatched area a. Since A remains constant while a increases, the obstruction ratio m also increases. It means that the discharge passing through the opening is decreasing.

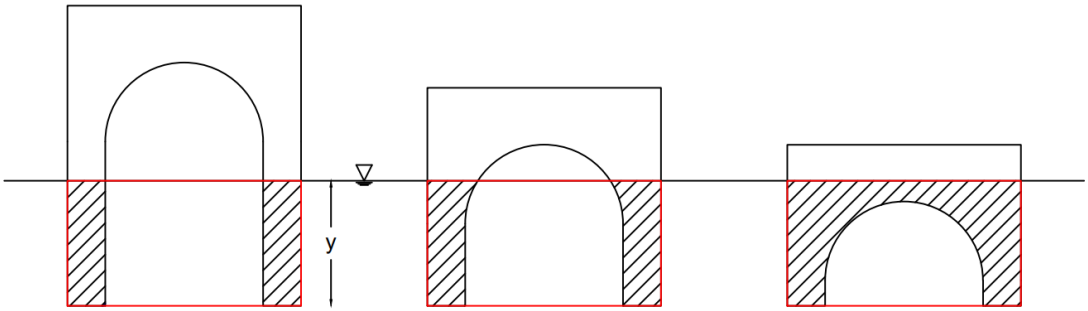

Figure 4.17: Three different cases of bridge obstruction ratio for abutment s=26, s=13 and s=5.

Using the software *Autocad*, it has been possible to calculate the areas a and A and consequently the obstruction ratio m for all the 9 tests, as reported in Tab. 4.4.

Table 4.4: Values of the obstruction ratio m for the 9 tests

s	**a** (m^2)	**A** (m^2)	$\boldsymbol{m}$ $(-)$
26	0.02376	0.07326	0.324
21	0.02376	0.07326	0.324
17	0.02380	0.07326	0.325
13	0.02460	0.07326	0.336
7	0.03120	0.07326	0.426
5	0.03620	0.07326	0.494
4	0.03870	0.07326	0.528
3	0.04120	0.07326	0.562
2	0.04226	0.07326	0.577

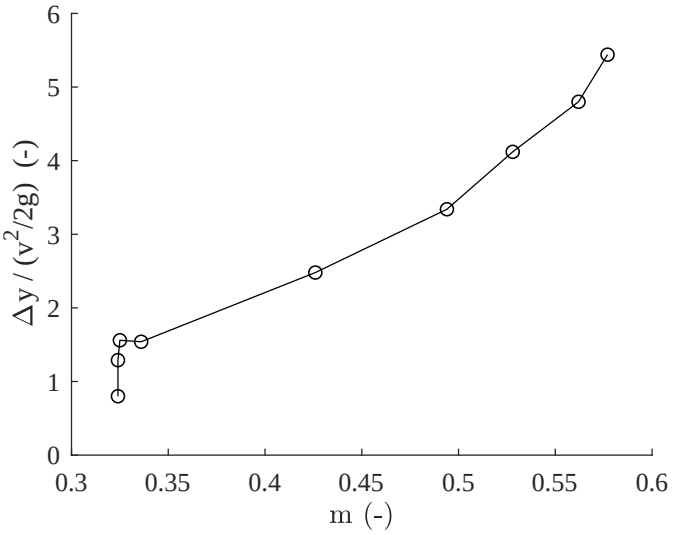

Figure 4.18: Dimensionless backwater plotting against the obstruction ratio m.

Fig. 4.18 displays the dimensionless backwater $(\Delta y)/(v^2/2g)$ against the obstruction ratio m. The points represent the selected tests with s decreasing low from bottom to top. In the dimensionless backwater, v is the tailwater velocity. As the bridge lowers, the backwater elevation and the obstruction ratio rise as shown in the graph.

Sub-critical to super-critical to sub-critical flow

The arch bridge case above mentioned offers the possibility to extend the scenario to another situation: the transition from sub-critical to super-critical flow and back to sub-critical flow. This situation could be very interesting to better understand the water flow passing through the bridge with a high discharge causing a different water behaviour. This simulation is comparable to a scenario during a flood event, that could take place in the urban part of Florence under extreme circumstances. The numerical setup for this case is the same as the one presented in the previous subsection. The main input changes regard the inlet and the outlet boundary conditions. The outlet boundary condition is fixed with a water level of y=0.198 m (the water level fixed for sub-critical flow in the previous case). The inlet boundary condition is determined with a higher discharge Q=0.300 m^3/s. Since the input and the setup of the model are the same, a higher discharge and a fixed water level at the end of the domain force the water to pass through the bridge narrowing, accelerating the flux (super-critical flow) and then decelerating with an hydraulic jump (sub-critical flow). In particular, two cases with different bridge abutments will be discussed: s=26 cm and s=13 cm. They represent two different situations with water level under and over the arches respectively.

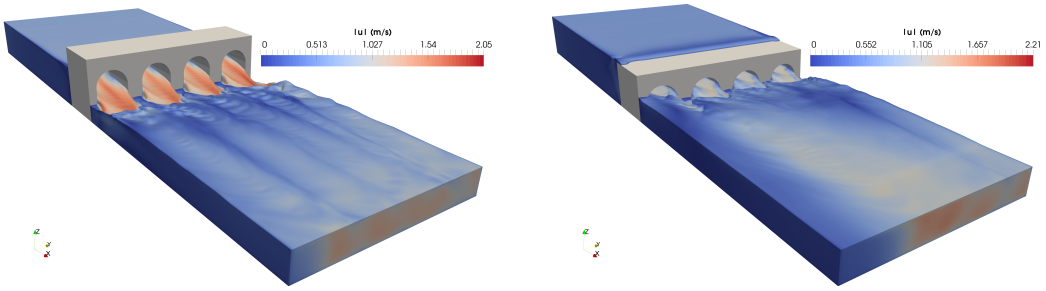

(a) *bridge abutment s=26 cm* (b) *bridge abutment s=13 cm*

Figure 4.19: Free surface with velocity magnitude contours for the arch bridge case in super-critical flow condition.

Fig. 4.19 shows the free surface features contoured by the velocity magnitude for the configurations above described. In particular, the water behaviour is well represented and easy to understand. The flow upstream the bridge is sub-critical. Then the bridge changes the conditions and the water adapts to pass through the bridge with a super-critical flow. Finally, the flow passes again to a sub-critical condition through an hydraulic jump. In this last phase, important energy losses are measured. Moreover, in the simulation on the right side (b), a slight overtopping appears as the flow depth is close to the height of the bridge. In order to have a numerical confirmation of the flow regimes, Tab. 4.5 reports the Fr values for both the simulations around selected points along the x axis: 1.55 m, 2.35 m and 3.20 m. In these spots, two sub-critical and one super-critical flow conditions are assumed. The table confirms the presumptions.

Table 4.5: Froude number values for both the simulations around three points: two for the sub-critical and one for the super-critical conditions.

	x (m)	**u** (m/s)	***y*** (m)	**Fr** $(-)$
s=26	1.55	0.64	0.32	0.361
	2.35	1.47	0.15	1.212
	3.20	0.29	0.20	0.207
s=13	1.55	0.51	0.37	0.268
	2.35	1.25	0.15	1.03
	3.20	0.67	0.21	0.467

The water surface lines, displayed in Fig. 4.20, help to focus on some details about the two simulations. The comparison between the two lines highlights different scenarios. In the simulation with the abutment s=26 cm, the water discharge can fully pass through the bridge arches. Subsequently the free surface is represented with two

different profiles $M2$ and $S2$ linked together by an hydraulic jump. In the simulation with the abutment s=13 cm, the bridge arches opening is not wide enough to allow the water discharge to pass through completely. Hence, the water level rises upstream the bridge as shown in Fig. 4.20. The free surface is represented with a profile $M1$ linked to a profile $S2$ by an hydraulic jump.

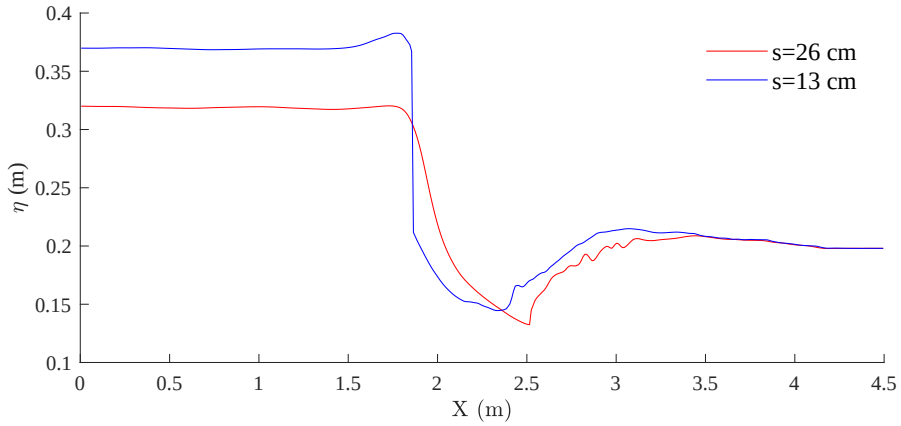

Figure 4.20: Water surface lines representing both the simulations for abutment s=26 and s=13.

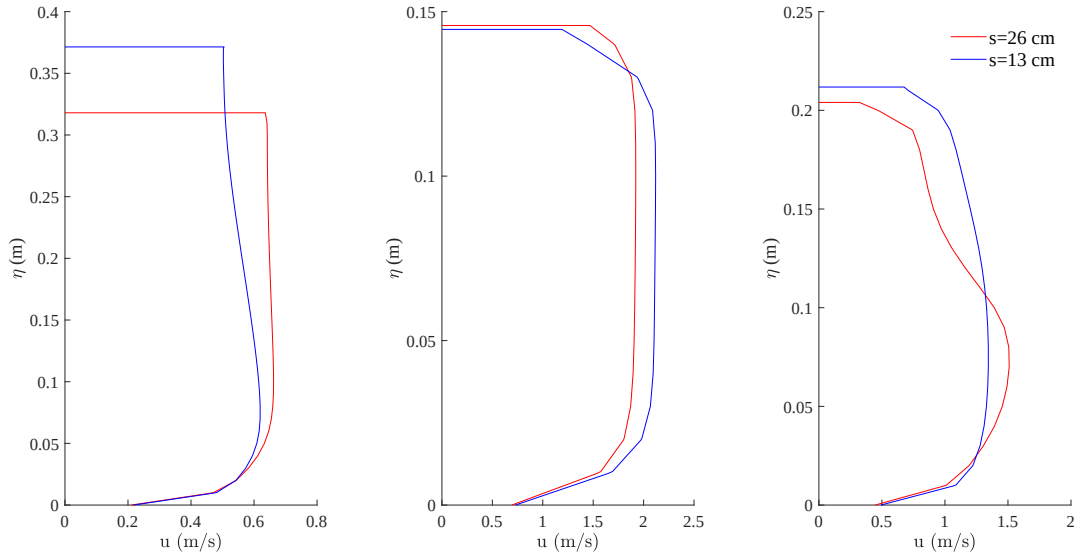

(a) $x = 1.55\ m$ (b) $x = 2.35\ m$ (c) $x = 3.20\ m$

Figure 4.21: Velocity profiles along the z-direction in selected points along the x axis.

In order to complete the case, Fig. 4.21 represents the velocity profiles along the

vertical axis. The points chosen for the measurements are the same: x=1.55 m, 2.35 m and 3.20 m. Every picture compares the velocity profiles for both simulations.

4.3 Arno: 2D Model

The first approach applied to the Arno river case is based on a two-dimensional model. Before introducing the simulation results, the model is briefly described.

4.3.1 Model characteristics

Since the present work deals with a river, the model solves the Shallow Water Equations (SWE). They are based on RANS equations but include further transformations and the following assumptions:

- hydrostatic distribution of pressure;
- altimetric velocity component (along z-axis) smaller than the longitudinal and transversal components (along x and y-axis);
- depth-averaged velocities in z-direction;
- small slope of the channel bottom.

In REEF3D, an additional term allows the user to include non-hydrostatic pressure.

4.3.2 2D Model Results

The two-dimensional simulation of the channel represents an important opportunity to understand the overall flow pattern of the river. Considering the approach as a qualitative analysis, the 2D model has also the aim to identify the areas where deeper investigation is needed and where the hydraulic phenomena are more complex. In this context, a three-dimensional simulation can provide more details.

For the present work, the 2D simulation time is set to 7200 s with a constant water discharge of 2000 m^3/s on the inlet. For the turbulence model, the k-ϵ approach is used. Fig. 4.22 displays the water flow and its interaction with the multiple infrastructures located along the river reach. More precisely, the figure represents the velocity pattern in x and y direction, in order to have an idea of the effects caused by the presence of the piers and the weir. The highest velocity, calculated during the

simulation, corresponds to 3.63 m/s.

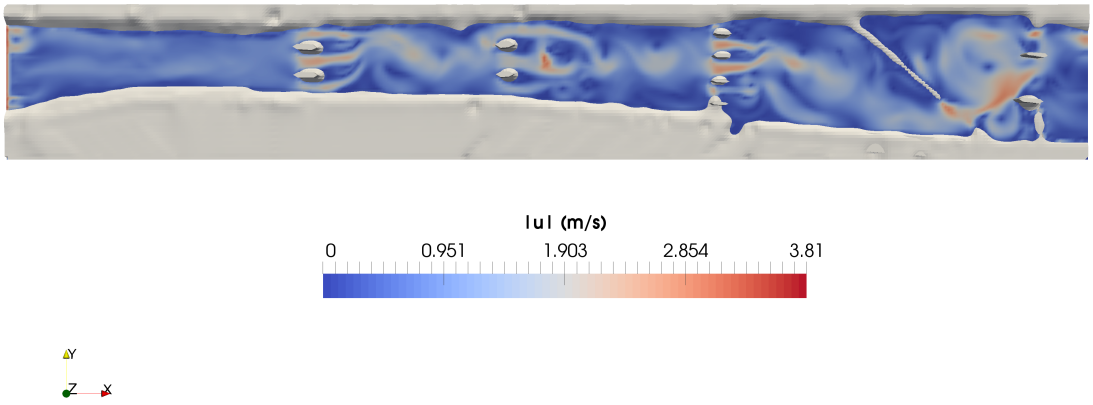

Figure 4.22: 2D simulation of the Arno river reach. In particular, the velocity magnitude along the domain is shown.

The scenario simulated and illustrated in Fig. 4.22 is a good representation of the real water flow. In fact, in proximity of the piers, where the cross section reduces its width, the flux lines change their direction and converge towards the gaps. In this situation, the flow regime, as analysed in subsection 4.1.1, becomes super-critical. The increase of the velocity vectors around the narrow section prove this phenomenon. Moreover, it is possible to notice that, in the valley side of the piers, small vortexes are created. In fluid dynamics this zone is called *wake*, the pressure values are negative and the presence of vortexes can caused damages to the back of the structures. Another important part of the simulation is represented by the oblique weir. Because of its particular position, as shown in Fig. 4.22, the flux lines change their direction towards the left side of the channel and create two recirculation zones characterised by vortexes. As reported in [4], this scenario reflects the real situation: the flux direction change leads to the erosion of the left pier of the Ponte Vespucci bridge while the vortex on the right side creates an important deposit zone.
Even if the simulation seems to respect the natural water behaviour along the river reach, it is not possible to consider it realistic, since an important parameter is not considered: the roughness. This parameter influences the fluid dynamic regime, the creation of the boundary layer and the velocity profiles near the walls. Hence, it is possible to use the present 2D model only to have a general idea of the flow pattern.

4.4 Arno: 3D Model

Finally, the 3D model of the Arno river has been created. In particular, three different situations have been analysed:

- Ponte Vecchio bridge with three different water discharges.
- Ponte Vecchio and Santa Trinita bridges with a 909 m^3/s water discharge.
- The whole river reach with a 909 m^3/s water discharge.

Every situation gradually involves bigger domains. This enables the creation of the model, step by step and helps to better identify problems during the simulations. Moreover, it is also possible to have an idea of the effects caused by the structures interacting together.
As already described, the 3D model of the Arno river represents the third and last step of the process for the model development. Hence, complex bottom and hydraulic structures are present.

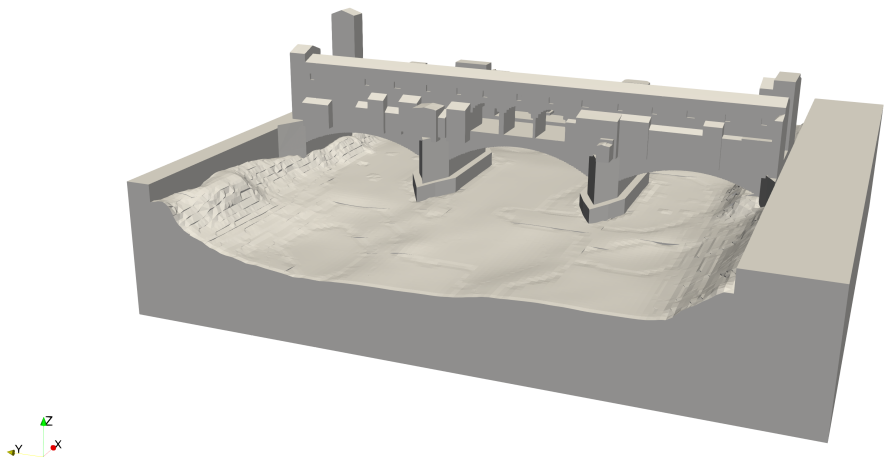

Figure 4.23: Complex bottom and hydraulic structure representing the river reach together with Ponte Vecchio bridge.

Fig. 4.23 shows only a part of the river reach including the Ponte Vecchio bridge. It can be noticed a good approximation of the complex bottom (from LIDAR and Multibeam surveys) and the complex structure (Ponte Vecchio) lying exactly on the river bed. The cells mesh is accurate and respects the reality. Erosion and deposit zones are clearly visible. The cell size chosen for all the simulations is dx=1.0 m. This size is the smallest that can be used with a good balance between accuracy,

number of cells and computational cost. One of the most essential aspects is expressed by the boundary conditions. A constant water discharge characterises the initial boundary condition. The outlet boundary condition is set as a controlled outflow with a fixed water level at the closure section. The water surface levels used for the outlet boundary conditions are provided by the 1D HEC-RAS simulation. This approach is used for all cases. Moreover, the results will be discussed and compared with the experimental data from the field measurements and from the 1D HEC-RAS simulation. Only in the case of the Ponte Vecchio bridge, the results will be compared with the Bologna scaled model data when higher discharges are used.

4.4.1 Ponte Vecchio Bridge

Ponte Vecchio bridge is the first situation analysed. The domain for this scenario has a 120 m length and a 120 m width. The bridge is placed 60 m downstream of the inlet, exactly in the centre of the domain. The natural river banks are represented by the topography data. Two supplementary walls are added at both sides of the river. Three different water discharges are used for the initial boundary condition: 909, 2600 and 3000 m^3/s. For each discharge, three water depths are investigated respectively: 43.7, 47 and 47.84 m. Hence, different water levels are obtained and it is possible to understand how the water raises and to compare the heights with three different discharges.
Fig. 4.24 and Fig. 4.25 show the free surface with the velocity magnitude contours for the upstream and the downstream of Ponte Vecchio bridge with a 909 m^3/s water discharge. The water is completely contained inside the banks and does not overflow the walls. Because of the bridge narrowing, the flux changes direction and is forced to pass through the spans. In these spots, the velocity of the flux is higher than the one before the bridge, following Bernoulli's law. Few meters after the piers, the flow is still influenced from the hydraulic structure. Hence, the velocity does not decrease and keeps constant on higher values until the end of the domain. Another important phenomenon is the wake caused by the structure on the back of the piers. The negative pressure zone is well simulated respecting the natural water behaviour. Other important details are clearly visible, for instance, the backwater in proximity of the piers upstream the bridge. The collision of the water with the piers causes a raising of the water levels, shown in Fig.4.24. In the same figure it is also possible to notice a strip along the piers (in x direction) where the velocity of the flow is very low. This aligns to the no-slip condition, regarding the interaction between a solid and a fluid. In particular, in fluid dynamics, this condition assumes that the fluid has zero velocity in proximity of a solid boundary. Going away from the boundary, the fluid velocity raises. Also the roughness and the boundary layer are strictly related to this phenomenon.

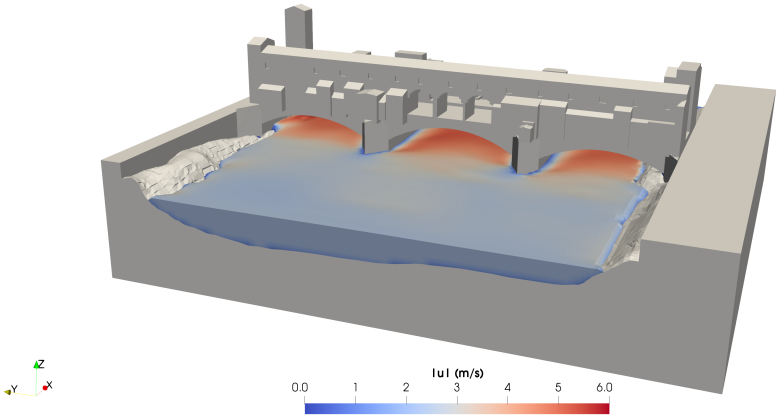

Figure 4.24: Free surface on the upstream side with velocity magnitude contours for Ponte Vecchio bridge with a 909 m^3/s water discharge.

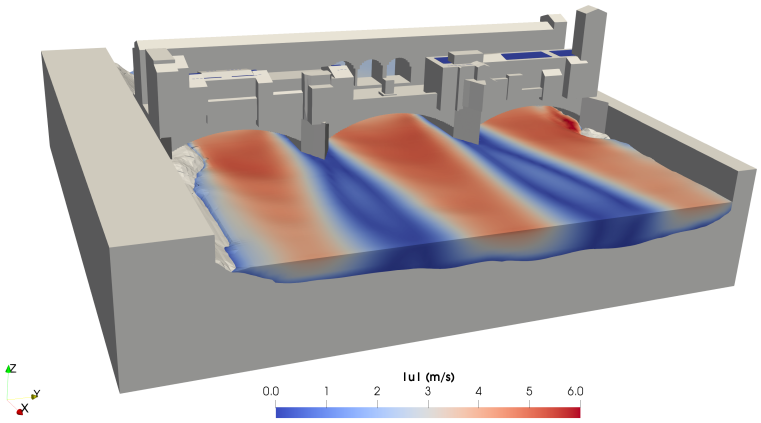

Figure 4.25: Free surface on the downstream side with velocity magnitude contours for Ponte Vecchio bridge with a 909 m^3/s water discharge.

In order to be able to evaluate the model, the results are compared with field measurements. Since the field data have been collected upstream and downstream around the centre of each bridge, only two points for each structure are available for comparison. Moreover, a line, passing through the central span, has been used to record the water levels of the simulation along the whole domain. Tab. 4.6 and Fig. 4.26 show the values and the graph of the water heights upstream and downstream the bridge respectively.

Table 4.6: Water surface levels upstream and downstream Ponte Vecchio bridge obtained from field measurements, HEC-RAS and REEF3D considering a 909 m^3/s discharge.

	Water Level (m $a.s.l.$)		
	Field Data	**HEC-RAS**	**REEF3D**
Upstream	43.43	43.77	43.39
Downstream	43.52	43.72	43.47

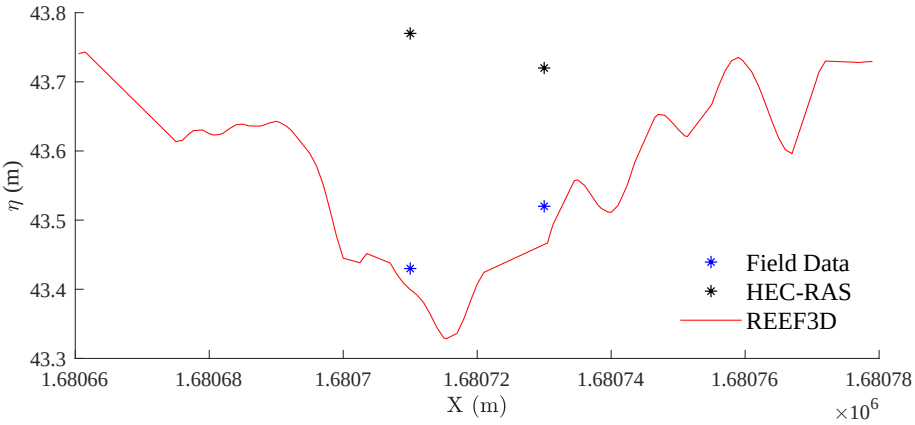

Figure 4.26: Water levels comparison between the field measurements, the HEC-RAS data and the results upstream and downstream of the Ponte Vecchio bridge with a 909 m^3/s water discharge along a line passing through the centre of the structure.

From the figure, it is possible to appreciate the slight difference between the field data and the results. The gap is fixed to 4 and 5 cm for the upstream and the downstream respectively. Hence, the results match the real data with success. The HEC-RAS values are quite far. Moreover, it can be noticed that the lowest water level is included between the upstream and the downstream of the bridge. This is in line with the hydrodynamic theory: the narrower the section the higher the velocity and the lower the height.
Another interesting aspect regards the regime of the flow. In these terms, the estimation of the Froude number Fr is very important. On the base of the results obtained from the simulation, Fr can be calculated only point by point. Two spots have been chosen: 20 m upstream and 10 m downstream the bridge. As shown in Tab. 4.7, both spots are characterised by Fr < 1, which means sub-critical flow.

Table 4.7: Froude number values for Ponte Vecchio bridge with a 909 m^3/s water discharge in two different points: A, 20 m upstream, and B, 10 m downstream the bridge.

	x (m)	**u** (m/s)	***y*** (m)	**Fr** $(-)$
A	1680690	2.65	5.64	0.357
B	1680740	5.19	4.50	0.781

For the sake of completeness, the velocity profiles are displayed for both points in Fig. 4.27. Even if the shape of the profiles is different, the velocity constantly increases starting from the river bed towards the free surface, where the value is the highest. This behaviour accords with the river dynamics.

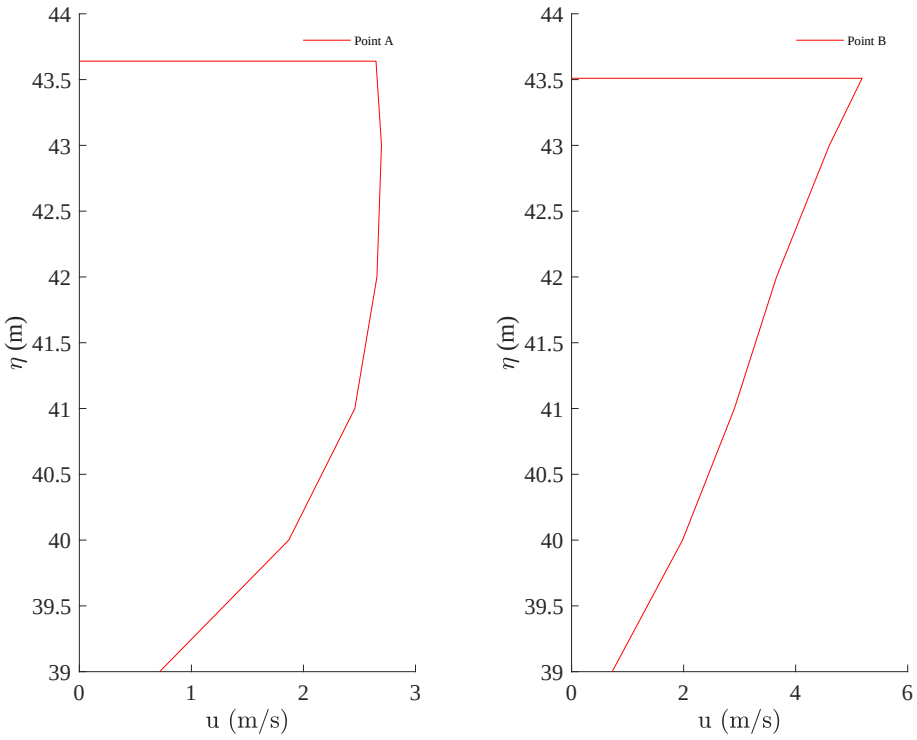

(a) *Point A (upstream)* (b) *Point B (downstream)*

Figure 4.27: Velocity profiles along the vertical axis in two different points A and B upstream and downstream the bridge respectively.

The other two situations for Ponte Vecchio bridge will be discussed in parallel. The main change regards the water discharge at the inlet: 2600 and 3000 $m3/s$.

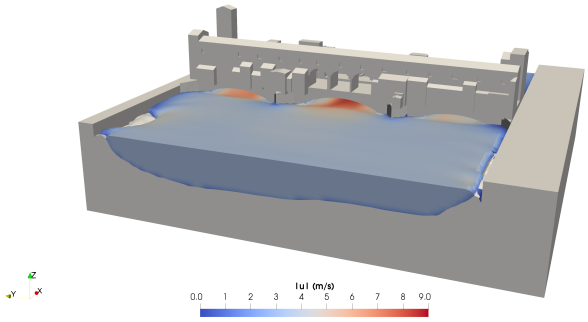

(a) *Q=2600* m^3/s

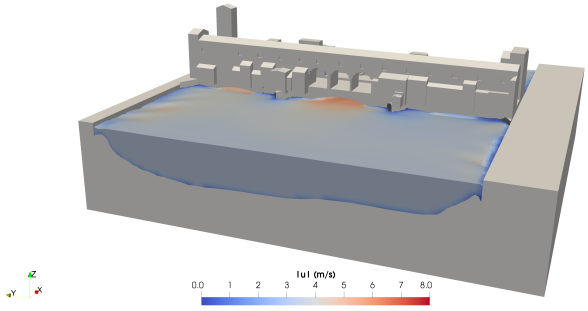

(b) *Q=3000* m^3/s

Figure 4.28: Free surface on the upstream side with velocity magnitude contours for Ponte Vecchio bridge with two different water discharges.

Fig. 4.28 shows again the free surface contoured with the velocity magnitude. Obviously, higher discharges lead to higher water levels. In both cases the great amount of water is completely confined by the walls. The dynamics of the river are the same described for the 909 m^3/s discharge but with more elevated heights. Also, the velocity values do not change along the domain, involving, in some points, higher peaks. The regime of the flow is sub-critical.
In order to evaluate the reliability of these last two cases, the numerical values (Tab. 4.8 and Tab. 4.9) and the graphs (Fig. 4.29 and 4.30) shown below correspond to each discharge. For these cases, besides the HEC-RAS data, only the experimental data from Bologna scaled model were available for the comparison with the results. Moreover, they are referred only to the bridge upstream.

Table 4.8: Water surface levels upstream Ponte Vecchio bridge obtained from Bologna scaled model experimental data, HEC-RAS and REEF3D considering a 2600 m^3/s discharge.

	Water Level (m $a.s.l.$)		
	Exp Data	**HEC-RAS**	**REEF3D**
Upstream	47.08	47.05	46.84

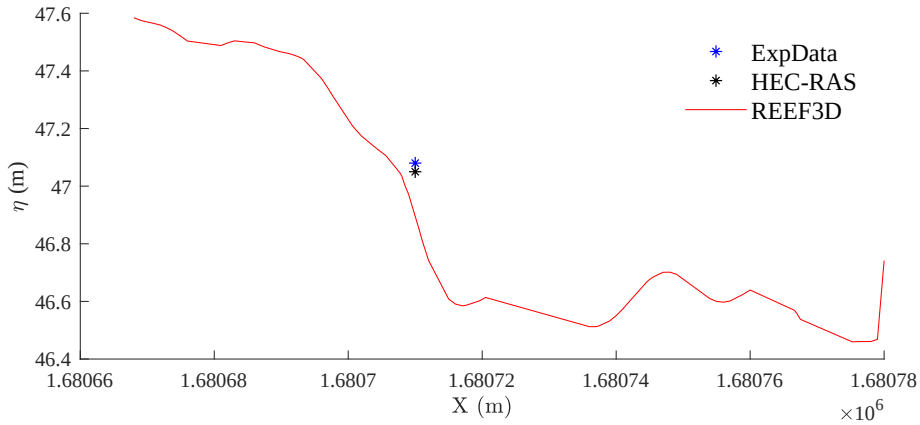

Figure 4.29: Water levels comparison between the field measurements, the HEC-RAS data and the results upstream and downstream Ponte Vecchio bridge with a 2600 m^3/s water discharge along a line passing through the centre of the structure.

Table 4.9: Water surface levels upstream Ponte Vecchio bridge obtained from Bologna scaled model experimental data, HEC-RAS and REEF3D considering a 3000 m^3/s discharge.

	Water Level (m $a.s.l.$)		
	Exp Data	**HEC-RAS**	**REEF3D**
Upstream	47.69	47.84	48.11

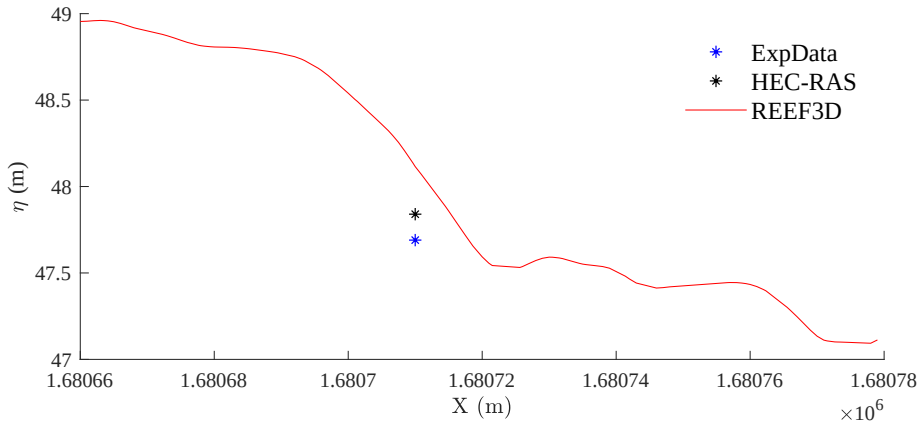

Figure 4.30: Water levels comparison between the field measurements, the HEC-RAS data and the results upstream and downstream Ponte Vecchio bridge with a 3000 m^3/s water discharge along a line passing through the centre of the structure.

In both cases, the accuracy of the results is less sufficient. The difference in the calculated water depths are 24 cm and 42 cm for the 2600 and the 3000 m^3/s discharges respectively compared to the experimental data. On the one hand, HEC-RAS is based on 1D simulations, which are quite far from the 3D precision of computation. On the other hand, the experimental data are obtained from a scaled model that could be influenced by scale effects, in particular in relation to small gaps. It is also possible that the large amount of water caused an overestimated raising of the levels. These conditions could lead to the discrepancies.
In order to complete the Ponte Vecchio case, Fig. 4.31 displays the three situations with the three different discharges highlighting the water level differences. For the two lower discharges, it can be noticed a free surface flow with completely open spans. Instead, the 3000 m^3/s water discharge causes a free surface flow on the left side, for the first two spans. The right span is submerged, so the flow is pressurised and the water level raises over the arch of the bridge.

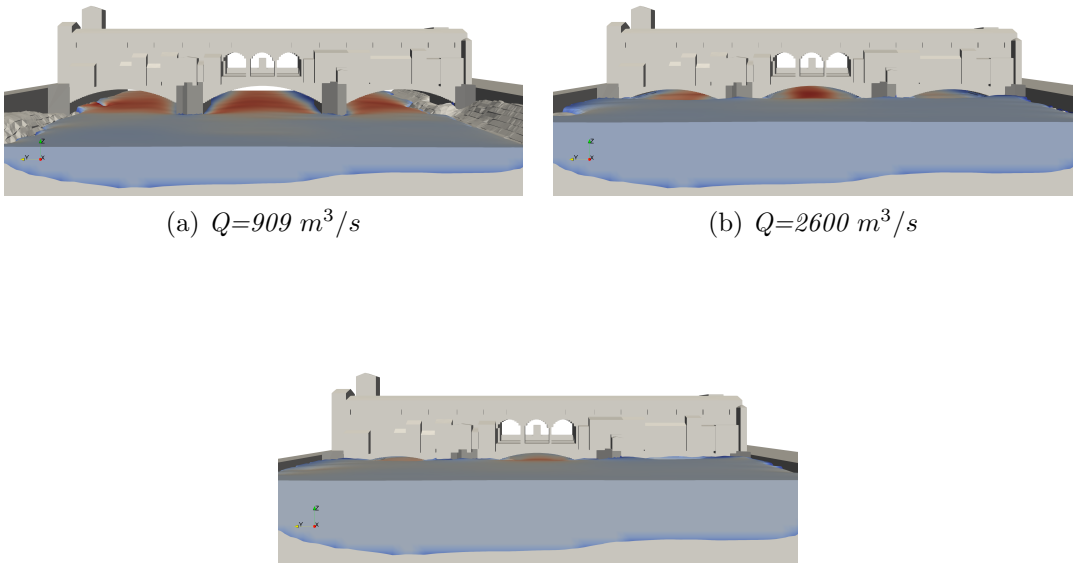

(a) *Q=909* m^3/s (b) *Q=2600* m^3/s

(c) *Q=3000* m^3/s

Figure 4.31: Water surface levels on the upstream side for Ponte Vecchio bridge for three different water discharges Q: 909, 2600 and 3000 m^3/s.

4.4.2 Ponte Vecchio and Santa Trinita Bridges

The second case regards a bigger domain in which Ponte Vecchio and Santa Trinita bridge are included. The area has a 400 m length, a 125 m width and a 43.6 m water depth. The bridges are placed 50 m after the inlet and 80 m before the outlet respectively with a 230 m gap in between. This distance allows the river to stabilise the flux after the hydraulic structure (Ponte Vecchio bridge) before passing through the next one (Santa Trinita bridge). This situation has been chosen for the simulation due to the hydrodynamic relation among the two structures. In fact, since they are quite close, during important flood events, the hydraulic situation of Santa Trinita bridge influences Ponte Vecchio bridge, in particular in relation to the backwater. For this case, only a 909 m^3/s water discharge has been simulated. Even if the discharge is low, it is possible to analyse the scenario and discuss the results. Fig. 4.32 shows the domain under investigation. As for the other cases, the figure highlights the velocity field.

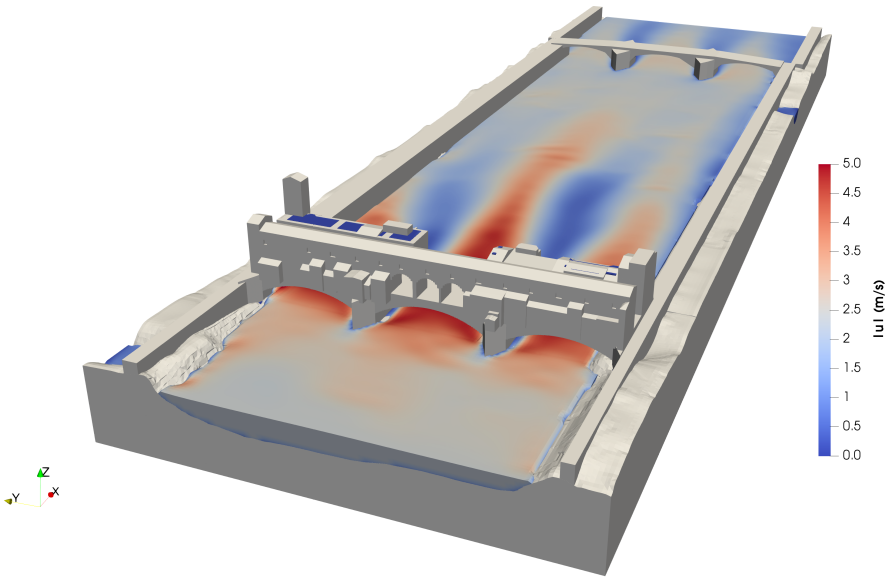

Figure 4.32: Free surface with velocity magnitude contours for Ponte Vecchio and Santa Trinita bridges with a 909 m^3/s water discharge. The near face of the image is the upstream side.

In general, the flow respects the dynamics of the river, with higher velocities in proximity of the bridges contractions, and lower velocities far from the structures and along the banks. In order to have more details, Tab. 4.10 and Fig. 4.33 show the numerical values and the comparison between the results, HEC-RAS, and the field data regarding the water levels.

Table 4.10: Water surface levels upstream and downstream Ponte Vecchio and Santa Trinita bridges obtained from field measurements, HEC-RAS and REEF3D considering a 909 m^3/s discharge.

Bridge	**Water Level** (m *a.s.l.*)		
	Field Data	**HEC-RAS**	**REEF3D**
Ponte Vecchio upstream	43.43	43.77	43.13
Ponte Vecchio downstream	43.52	43.72	43.00
Santa Trinita upstream	43.16	43.49	43.27
Santa Trinita downstream	43.10	43.46	43.29

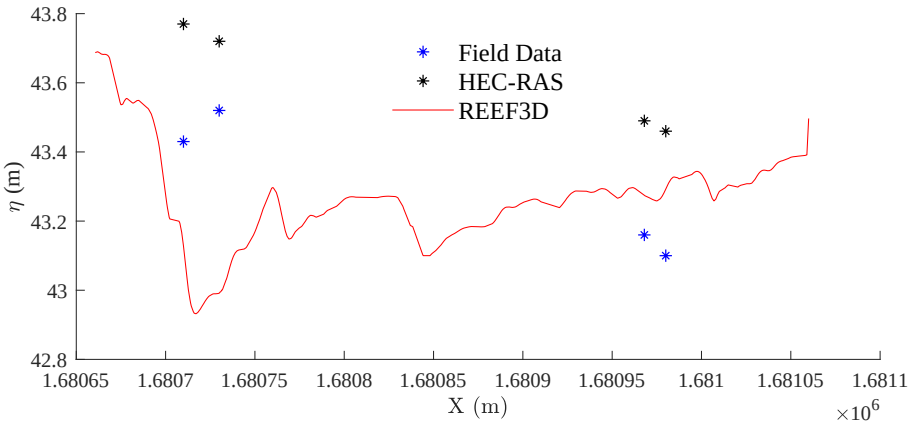

Figure 4.33: Water levels comparison between the field measurements, the HEC-RAS data and the results upstream and downstream Ponte Vecchio and Santa Trinita bridges with a 909 m^3/s water discharge along a line passing through the centre of the structure.

The results do not exactly match the field data, but they are quite accurate. Excluding the downstream of Ponte Vecchio bridge, the results are closer to the field data than HEC-RAS. The simulation can be considered satisfactory. The only exception is the water level recorded around Ponte Vecchio bridge downstream, where a very low height is simulated. In theory, because of the backwater from Santa Trinita bridge, the water should be higher as in the single Ponte Vecchio bridge case. Probably, changing the input at the outflow, could have influenced the simulation.

4.4.3 Total Simulation

The last case considered for the Arno river is the whole domain including the four bridges (Ponte Vecchio, Santa Trinita, alla Carraia, Vespucci) and the weir (Pescaia di Santa Rosa). The area has a 1400 m length, a 200 m width and a 43.9 m water depth. The river reach under investigation is very extended. The number of cells (considering a mesh size dx=1 m) is around 10 millions. The water discharge used for the simulation is 909 m^3/s. Using this discharge, it is possible to compare the results with the field measurements collected during a real event.
Fig. 4.34 shows a plan view of the river reach that can be useful to understand the water behaviour and the flux direction. It is very important to keep in mind that three new hydraulic structures (two bridges separated by a weir) can influence part of the simulation. Analysing the figure, the flow respects the fluid dynamics laws. In particular, in proximity of the bridges, the velocities increase and then decrease after the contraction. The last section of the domain is characterised by the weir and the Vespucci bridge. Over the weir, the flow should accelerate, follow the shape of

the weir and then generate a hydraulic jump (due to a lowering of the river bottom). Watching with attention Fig. 4.34, it seems the velocities slightly increase over the weir, without the hydraulic jump downstream the structure. Fig. 4.35 helps to understand more in depth the hydrodynamic situation. The three-dimensional view makes possible to focus on some details, in particular the water levels. After crossing the weir, the water height does not lower and the free surface is flat.

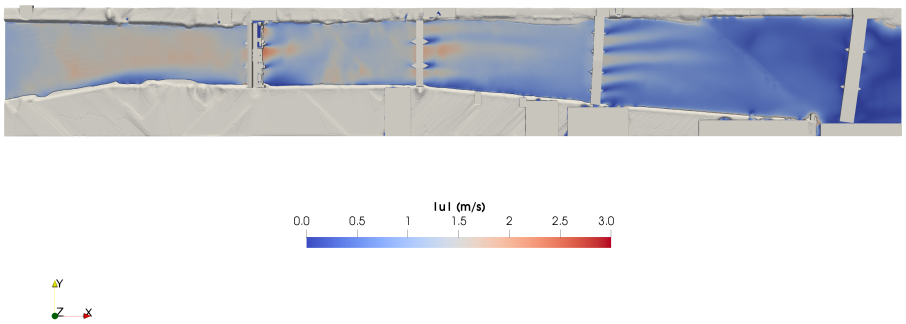

Figure 4.34: Plan view of the whole river reach. In particular free surface with velocity magnitude contours with a 909 m^3/s water discharge.

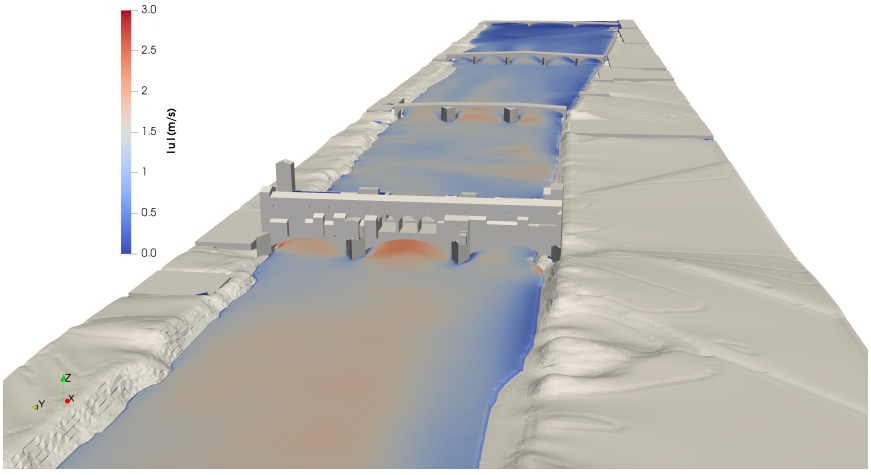

Figure 4.35: Free surface seen from the upstream side with velocity magnitude contours for the whole river reach with a 909 m^3/s water discharge.

In order to make the situation clearer, Tab. 4.11 and Fig. 4.36 display the numerical and graphical results obtained from the simulation in comparison with the field

and HEC-RAS data. As analysed above, the flow respects the river dynamics until alla Carraia bridge. Hence, the results match with slight gaps. In particular, Santa Trinita bridge has a difference of only 3 and 2 cm with the field data, upstream and downstream the bridge respectively. Since it was not possible to collect field measurements for the weir, the last section can be analysed on the basis of the Vespucci bridge. As shown in the graph, the discrepancy between the results and the field data is very important. More exactly, an almost 4 m large gap is recorded upstream and downstream of the bridge. For this reason, the total simulation of the river cannot be considered reliable and further analyses is avoided. Instead, it is important to understand the reasons that caused this wrong representation of the weir. Probably, the extended domain, the complexity of the data and the outlet boundary conditions could have influenced the simulation. Moreover, the cell size should be decreased in further investigations because a higher number of cells lead to more details.

Table 4.11: Water surface levels upstream and downstream the four bridges along the river reach obtained from field measurements, HEC-RAS and REEF3D considering a 909 m^3/s discharge.

Bridge	**Water Level** (m *a.s.l.*)		
	Field Data	**HEC-RAS**	**REEF3D**
Ponte Vecchio upstream	43.43	43.77	43.98
Ponte Vecchio downstream	43.52	43.72	43.94
Santa Trinita upstream	43.16	43.49	43.13
Santa Trinita downstream	43.10	43.46	43.12
alla Carraia upstream	42.98	43.29	43.30
alla Carraia downstream	42.86	43.26	43.29
Vespucci upstream	39.64	40.11	43.79
Vespucci downstream	39.61	40.10	43.80

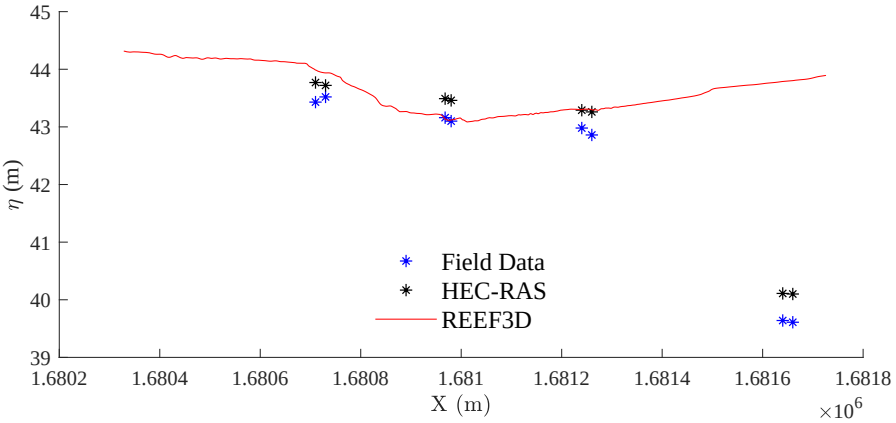

Figure 4.36: Water levels comparison between the field measurements, the HEC-RAS data and the results upstream and downstream the whole domain with a 909 m^3/s water discharge along a line passing through the centre of the structures.

A final comment shall be given about the flow regime of the river. Without considering the last section of the domain, the data recorded during the simulation confirm a Froude number of Fr < 1 which is in total agreement with the real flux.

Chapter 5

Conclusions

The main objectives of the present work are investigating the stability of the old structures of the Arno river in Florence and to reduce the high hydraulic risk in its urban part. In order to develop this complex analysis, the open-source hydrodynamic software REEF3D is applied to the real case of the urban reach of the Arno river. The software can deal with a wide range of applications within marine and hydraulic engineering. In particular two flow modules were used:

- REEF3D::SFLOW for two-dimensional simulations.
- REEF3D::CFD for three-dimensional simulations.

The data, provided by the Civil and Environmental Engineering Department of Florence, represents the basis on which the model is built.
Because of the complexity of the data and the structures used for the simulations, the model is created gradually, from simple to more elaborated situations. The first step consists in the analysis of two cases: the double pier and the weir, characterised by flat bottom and non complex structures. The numerical setup for both scenarios is based on the experiments by Szydlowski (2011) for the double pier and by Sarker and Rhodes (2004) for the weir respectively. Besides representing the first step for the model creation, these cases are also used for the software validation. In order to determine the appropriate cell size for the simulations, a grid convergence study is conducted. Then, for the simulation validation, the results are compared with the experimental data, and the findings highlighted the good correspondence of the points. Both simulations involve hydraulic jumps and two or three changes of flow regime respectively. Hence, the results agree well with the experiments.
The following step for the creation of the model considers the flow around an arch bridge, reproduced in the experiments by Vide and Prio (2005). Here, the bottom is still flat, while the hydraulic structure represents a complex shape. In fact, the case considers a bridge with semicircular arches. Since the shape of the bridge is inspired

by the Roman and medieval times, this case arouses great interest, in particular in relation to the Ponte Vecchio bridge. As for the validation cases the results are compared with the experimental data, in order to verify the correspondence with real measurements. The experiment is focused on the backwater caused by the hydraulic structure gradually lowering the bridge height. The results are affected by a slight discrepancy compared to the experimental data. However, the difference is reasonable. Moreover, in order to test the reliability of the results, the trend lines assume a very similar behaviour. Since the regime of the flow is established as sub-critical, the case has been extended to a new scenario in the context of this work, which is not studied in the experiments by Vide and Prio (2005). When changing the discharge of the initial boundary condition, the flow passes from sub-critical to super-critical condition in proximity of the bridge, and then again to sub-critical after the obstacle. The analysis, carried out from the results, in relation to the Froude number Fr, confirms the change of regime flow and enables the reproduction of the velocity profiles in selected points.

Before the last step a two-dimensional model is created in order to obtain a qualitative analysis. The purpose is to understand more in depth the overall pattern of the river and the orientation of the flux lines. The simulated scenario is a good representation of the real water behaviour. In fact, hydrodynamic phenomena like increasing of velocities around the section narrowings and wake zones on the back of the piers occurred during the simulation. Recirculation zones are represented in accordance with reality. However, even if the simulation seems to respect the natural flow of the river, the roughness is not included. Therefore the simulation cannot be considered realistic since the roughness represents one of the most important hydraulic parameters.

Finally, the last step leads to the creation of the Arno river model. The complexity of the bottom given by the topography, as well as the detailed shape of the structures represent a significant challenge for the success of the model simulation. In order to identify possible problems, the case has been divided in three sub-cases, gradually involving bigger domains. For each sub-case the water discharge of 909 m^3/s is used for the inflow boundary condition and the water level (from the 1D HEC-RAS simulation) is fixed for the outflow boundary condition. Moreover, for the selected discharge, field measurements of the water levels are available to compare to the simulation results. The first sub-case regards the Ponte Vecchio bridge. The velocity contours highlight how the flow behaves when the cross section reduces because of the bridge: the velocities in proximity of the narrowing increase, whereas they decrease downstream the bridge. Also the backwater (when the flow collided the piers upstream) and the no slip condition (along the piers) are obtained in the simulation in accordance with the fluid dynamics theory. Afterwards, the results obtained for the water levels are compared with field measurements and the HEC-RAS data, re-

vealing a good matching with the field data. Two points are selected to investigate the Froude number, confirming a sub-critical flow. Only for Ponte Vecchio bridge, two higher discharges are used: 2600 and 3000 m^3/s. In these two situations, the results are not completely accurate. In defense of the results, the data used for the comparison are obtained from the Bologna scaled model experiments and could be influenced by scale effects. However, the comparison between the three situations with different discharges, helps to understand the raising of the water levels and the possible water volume contained into the banks.
The second sub-case involves a bigger domain including Ponte Vecchio and Santa Trinita bridges. Since the bridges are quite close, the objective is to better understand the relationship between the two structures. In fact, comparing the water levels from the simulations with the field data, Santa Trinita bridge influences Ponte Vecchio bridge recording different values from the previous sub-case. The results do not match fully the data, but they represent a good approximation.
The third sub-case includes the whole domain, from Ponte Vecchio bridge to Vespucci bridge, for a total length of 1.4 km. The flow respects the fluid dynamics theory: in proximity of the section narrowings the velocities increased, while, after the hydraulic structures, the velocities decreased again. The flow is well represented in the simulation until the weir, called Pescaia di Santa Rosa. In correspondence of this point the water does not follow the weir creating an hydraulic jump, but remains constant and flat. While, before the weir, the water levels match with a good accuracy the field measurements, after the weir, the discrepancy is higher. For this reason, the total simulation has to be investigated further. The chosen cell size is coarse with respect to the large domain size of the domain, the complexity of the data as well as the boundary conditions chosen are possible causes for these deviations.

The present work can be considered as a good starting point to better understand the dynamics of the flow regarding the urban part of the Arno river in Florence. Some important fluid dynamics concepts were addressed, clarifying some hydraulic issues. REEF3D helped to reproduce very complicated phenomena from both laboratories and reality, showing important and powerful features, even if some problems occurred. In general, the CFD approach represents the best way to follow, and the main tool that allows the engineer to identify possible solutions for hydraulic challenges.

Bibliography

[1] David Adalsteinsson and James A Sethian. A fast level set method for propagating interfaces. *Journal of computational physics*, 118(2):269–277, 1995.

[2] Nadeem Ahmad, Hans Bihs, Dag Myrhaug, Arun Kamath, and ivind A. Arntsen. Three-dimensional numerical modelling of wave-induced scour around piles in a side-by-side arrangement. *Coastal Engineering*, 138:132 – 151, 2018.

[3] J Anderson, John David and Wendt. *Computational fluid dynamics*. 1995.

[4] Daniele Bartolozzi and Alberto Caciolli. *Indagine sperimentale sul fenomeno di erosione localizzata alla pila sinistra del Ponte Vespucci nel Fiume Arno a Firenze*. PhD thesis, School of Florence, 2016.

[5] Petter A. Berthelsen and Odd M. Faltinsen. A local directional ghost cell approach for incompressible viscous flow problems with irregular boundaries. *Journal of Computational Physics*, 227(9):4354–4397, 2008.

[6] H. Bihs and A. Kamath. A combined level set/ghost cell immersed boundary representation for floating body simulations. *International Journal for Numerical Methods in Fluids*, 83(12):905–916, 2017.

[7] Hans Bihs, Arun Kamath, Mayilvahanan Alagan Chella, Ankit Aggarwal, and Øivind A. Arntsen. A new level set numerical wave tank with improved density interpolation for complex wave hydrodynamics. *Computers and Fluids*, 140:191–208, 2016.

[8] Enrica Caporali, Massimo Rinaldi, and Nicola Casagli. The Arno River Floods. *Giornale di Geologia Applicata*, 1(November 1966):177–192, 2005.

[9] Alexandre Joel Chorin. Numerical solution of the navier-stokes equations. *Mathematics of computation*, 22(104):745–762, 1968.

[10] Bernardo De Bernardis and Nicola Casagli. Fragilità del suolo e gestione degli eventi estremi, dalla cultura dell'emergenza a quella del suolo. *Ecoscienza*, 3:32–35, 2015.

[11] Università di Bologna. Studio su modello idraulico del regime di piena del fiumeArno entro la città di Firenze, nel tratto compreso tra il ponte Alle Grazie e la traversa S.Rosa. Technical report, Università degli Studi di Bologna, 1972.

[12] Robert D. Falgout and Ulrike Meier Yang. hypre: A Library of High Performance Preconditioners. pages 632–641, 2002.

[13] G Galloway, G Seminara, G Blöschl, M Garcia, A Montanari, and L Solari. *Saving a World Treasure: Protecting Florence from Flooding.* 2016.

[14] Erlend Liavg Grotle, Hans Bihs, and Vilmar sy. Experimental and numerical investigation of sloshing under roll excitation at shallow liquid depths. *Ocean Engineering*, 138:73 – 85, 2017.

[15] L. Hamill. *Bridge Hydraulics*, volume 127. 2001.

[16] Ami Harten. High resolution schemes for hyperbolic conservation laws. *Journal of Computational Physics*, 49(3):357–393, 1983.

[17] G S Jiang and C W Shu. Efficient implementation of weighted WENO schemes. *Journal of Computational Physics*, 126(126):202–228, 1996.

[18] Arun Kamath. *CFD based Investigation of Wave-Structure Interaction and Hydrodynamics of an Oscillating Water Column Device*, volume 3. 2015.

[19] Arun Kamath, Mayilvahanan Alagan Chella, Hans Bihs, and Øivind A. Arntsen. Evaluating wave forces on groups of three and nine cylinders using a 3D numerical wave tank. *Engineering Applications of Computational Fluid Mechanics*, 9(1):343–354, 2015.

[20] Arun Kamath, Mayilvahanan Alagan Chella, Hans Bihs, and Øivind A. Arntsen. Breaking wave interaction with a vertical cylinder and the effect of breaker location. *Ocean Engineering*, 128(September):105–115, 2016.

[21] Arun Kamath, Hans Bihs, Mayilvahanan Alagan Chella, and ivind A. Arntsen. Upstream-cylinder and downstream-cylinder influence on the hydrodynamics of a four-cylinder group. *Journal of Waterway, Port, Coastal, and Ocean Engineering*, 142(4):04016002, 2016.

[22] Arun Kamath, Mayilvahanan Alagan Chella, Hans Bihs, and Øivind A. Arntsen. Energy transfer due to shoaling and decomposition of breaking and non-breaking waves over a submerged bar. *Engineering Applications of Computational Fluid Mechanics*, 11(1):450–466, 2017.

[23] J. P. Martín-Vide and J. M. Prió. Backwater of arch bridges under free and submerged conditions. *Journal of Hydraulic Research*, 43(5):515–521, 2005.

[24] Muk Chen Ong, Arun Kamath, Hans Bihs, and Mohammad Saud Afzal. Numerical simulation of free-surface waves past two semi-submerged horizontal circular cylinders in tandem. *Marine Structures*, 52:1 – 14, 2017.

[25] Enio Paris, Simona Francalanci, Pina Nicoletta D E Cicco, Luca Solari, and Vieri Gonnelli. LA CONOSCENZA PER LA PREVENZIONE DEL RISCHIO IDRAULICO : il monitoraggio del Fiume Arno a 50 anni dall ' alluvione del 1966. pages 9–32, 2016.

[26] Ilario Principe and Paolo Sica. L'inondazione di Firenze del 4 Novembre 1966. *L'universo*, 2:192–222, 1967.

[27] Chi-Wang Shu. Total-variation-diminishing time. 9(6):1073–1084, 1988.

[28] Chi-Wang Shu. High-order Finite Difference and Finite Volume WENO Schemes and Discontinuous Galerkin Methods for CFD. *International Journal of Computational Fluid Dynamics*, 17(2):107–118, 2003.

[29] Mark Sussman, Peter Smereka, and Stanley Osher. A level set approach for computing solutions to incompressible two-phase flow. *Journal of Computational Physics*, 114(1):146 – 159, 1994.

[30] Dragica Vasileska. Poisson equation solvers, Jun 2010.

[31] D. Vetsch, A. Siviglia, D. Ehrbar, M. Facchini, S. Kammerer, A. Koch, S. Peter, L. Vonwiller, M. Gerber, C. Volz, D. Farshi, R. Mueller, P. Rousselot, R. Veprek, and R Faeh. *System Manuals of BASEMENT, Version 2.7*. 2017.

[32] Wikipedia. Alluvioni del fiume arno — wikipedia, l'enciclopedia libera, 2011. [Online; checked 21st June 2018].

[33] Wikipedia. Arno — wikipedia, l'enciclopedia libera, 2011. [Online; checked 21st June 2018].

[34] David C. Wilcox. *David C. Wilcox-Turbulence Modeling for CFD (Third Edition) -Dcw Industries, Incorporated (2006).pdf*. 2006.